

Landscape of Supersymmetric Particle Mass Hierarchies in Minimal Supergravity and Deflected Mirage Mediation Models

Baris Altunkaynak and Brent D. Nelson

Department of Physics, Northeastern University, Boston, MA, 02115 USA

Lisa L. Everett and Yongyan Rao

Department of Physics, University of Wisconsin, Madison, WI 53706, USA

Ian-Woo Kim

Department of Physics, University of Michigan, Ann Arbor, MI 48109, USA

Department of Physics, University of Wisconsin, Madison, WI 53706, USA

ABSTRACT: We study the landscape of supersymmetric particle mass hierarchies for the lightest four new states in the MSSM for two models of the soft supersymmetry breaking parameters: (i) minimal supergravity (mSUGRA), building on previous studies of Feldman, Liu, and Nath, and (ii) deflected mirage mediation (DMM), a string-motivated scenario in which the soft terms include comparable contributions from gravity mediation, gauge mediation, and anomaly mediation. In deflected mirage mediation, there is a wide variety of phenomenologically preferred models with light charginos, including novel patterns in which the heavy Higgs particles are lighter than the lightest superpartner.

Contents

1. Introduction	1
2. Theoretical Background	2
3. Methodology and Bounds	6
4. Hierarchy Patterns	10
4.1 Impact of Progressive Cuts	10
4.2 Hierarchy Patterns in mSUGRA and DMM	15
4.3 DMM Hierarchy Patterns: Parameter Space and Mass Spectra	20
5. Summary and Conclusions	33
A. DMM Parameters	36

1. Introduction

In the next decade, the hypothesis that physics beyond the Standard Model (SM) is given by TeV-scale softly broken supersymmetry (for reviews, see [1, 2]) will soon face unprecedented experimental tests at the Large Hadron Collider (LHC). These tests will have important implications for the supersymmetry breaking sector of these theories, which include the minimal supersymmetric standard model (MSSM) and its extensions. The parameter space associated with supersymmetry breaking is known to be vast; under the general (and phenomenologically preferable) assumptions of minimal flavor violation and CP conservation, there are approximately 30 parameters in the MSSM that are expected to be of relevance for collider physics. The standard approach to cope with this issue is to build theoretical models of the supersymmetry breaking terms and select benchmark parameter points, as in e.g. [3]. An alternative approach is to perform a general analysis of this approximately 30-dimensional parameter space, as was done recently by Berger *et al.* [4].

Within either approach, a recent strategy for studying supersymmetric models has been to consider the landscape of phenomenologically allowed mass patterns of the lightest four new particles (superpartners and/or additional Higgs states) of the theory, since it is these particles that are likely to be of relevance for collider physics. This strategy was advocated for minimal supergravity (mSUGRA) models (and other supergravity models) by Feldman, Liu, and Nath (FLN) in a series of papers [5, 6, 7], and has also been employed in the general MSSM [4]. The FLN analyses showed that even in minimal supergravity, there is a significant diversity of possible mass hierarchy patterns among the lightest four

states, which in turn results in a broader diversity of collider phenomenology than might have been anticipated by considering standard benchmark scenarios.

Motivated by the utility of this strategy, in this paper we provide a similar landscape study in which we compare the allowed light mass hierarchy patterns from minimal supergravity models with *deflected mirage mediation* (DMM) models [8, 9, 10]. Our primary focus is on deflected mirage mediation, a “mixed” supersymmetry breaking scenario in which the three standard mediation mechanisms – gravity mediation, gauge mediation, and anomaly mediation – are all present and provide comparable contributions to the soft breaking terms. Recent phenomenological studies of deflected mirage mediation, which is a generalization of mirage mediation [11, 12, 13], can be found in [14, 15, 16].

In our analysis, we follow the general procedure of FLN and enumerate the light mass hierarchy patterns for both mSUGRA and DMM models after imposing a series of phenomenological bounds. The cuts include current direct collider bounds on the superparticles and Higgs bosons, indirect bounds (including the updated bound on $B_s \rightarrow \mu^+ \mu^-$), and several options for the dark matter constraints, including the most recent bounds from WMAP7. Our mSUGRA results thus represent an update to the FLN results based on current phenomenological bounds. The DMM results show several striking differences between the preferred patterns found in mSUGRA, including the emergence of a dark matter-preferred pattern in which the lightest superpartner (LSP) is a “well-tempered”/mixed composition neutralino and the heavy Higgs bosons are lighter than the LSP, a pattern which is essentially absent in minimal supergravity models. We also find, most notably, that stop next-to-lightest superpartner (NLSP) patterns are strongly disfavored in DMM models, though otherwise there is a much wider variety of significant hierarchy patterns than is present in mSUGRA models.

This paper is structured as follows. We begin with a brief review of minimal supergravity and deflected mirage mediation, and describe our methodology. We then present our results, beginning with a presentation of the most prevalent light mass hierarchy patterns for a variety of dark matter constraints and Higgs bounds. We next discuss the patterns and characterize the associated model parameter space, focusing on the most prominent hierarchy patterns. Finally, we turn to our summary and conclusions.

2. Theoretical Background

We consider two classes of models, minimal supergravity and deflected mirage mediation. The two scenarios have the common feature that with certain assumptions, they satisfy the general criteria of minimal flavor violation (MFV) and CP conservation, such that the relevant soft breaking terms have the following general forms at the electroweak scale:

- Gaugino masses: M_a , $a = 1, 2, 3$.
- Third generation trilinear couplings: A_t , A_b , and A_τ .
- Third generation scalar masses: $m_{Q_3}^2$, $m_{u_3}^2$, $m_{d_3}^2$, $m_{L_3}^2$, and $m_{e_3}^2$.
- Light generation scalar masses: m_Q^2 , m_u^2 , m_d^2 , m_L^2 , and m_e^2 .

- Higgs scalar masses $m_{H_u}^2, m_{H_d}^2$.

In this work, we neglect the Yukawa couplings of the light generations and the neutrino sector. We also follow standard procedure and fix the magnitude of the supersymmetric Higgs mass parameter μ and the associated soft supersymmetry breaking term $b = B\mu$ in terms of m_Z and $\tan\beta$. Throughout our analysis, we will fix the sign of μ to be positive ($\mu > 0$), in accordance with the first study of FLN [5].

Minimal supergravity models are particularly straightforward models of this type. In mSUGRA models, supersymmetry breaking is assumed to arise in the observable sector at the traditional grand unification (GUT) scale of $M_G = 2 \times 10^{16}$ GeV. As is well known, the soft breaking terms are fixed at M_G by the following mSUGRA mass parameters:

- A unified gaugino mass, $m_{1/2}$
- A unified scalar mass, m_0
- A unified trilinear scalar coupling A_0 ,

as well as the value of $\tan\beta$ and the sign of μ . The mass parameters m_0 and $m_{1/2}$ range from the electroweak to TeV scale, while A_0 can range from zero to the TeV scale. The soft breaking terms take on the general forms described above upon renormalization group evolution to the electroweak scale. The resulting low energy phenomenology within mSUGRA models has been studied extensively in the literature (see e.g. the reviews [1, 2]).

Deflected mirage mediation models have several features that are quite different from mSUGRA models. One primary difference is that the parameters are generically non-universal at the GUT scale, and another is that the scenario involves an additional scale, which is the messenger scale associated with gauge mediation. Under certain assumptions, deflected mirage mediation models can obey MFV and CP conservation. To see this more clearly, we now provide a brief overview of DMM (see [8, 9, 16] for further details).

DMM models are string-motivated supergravity theories in which gravity mediation, anomaly mediation, and gauge mediation all provide comparable contributions to the soft terms. The scenario is motivated by the Kachru-Kalosh-Linde-Trivedi (KKLT) [17] approach to moduli stabilization in Type IIB string theory and the resulting phenomenological scenario of mirage mediation [11], in which it was demonstrated that the anomaly-mediated terms are comparable to the gravity-mediated terms resulting from the Kähler modulus associated with the compactification volume. Deflected mirage mediation generalizes mirage mediation to include effects of gauge mediation, which occur due to the generic presence of an additional SM gauge singlet that couple to vectorlike messenger pairs. As shown in [8, 9], depending on the details of the stabilization of this singlet, the resulting gauge-mediated terms can be comparable to the anomaly-mediated and modulus/gravity-mediated terms.

Deflected mirage mediation derives its name, as does mirage mediation, from the phenomenon that the gauginos appear to unify not at the GUT scale, but at a lower scale called the mirage unification scale (in mirage mediation, this also occurs for the scalar masses). The “deflection” of DMM models results from the fact that the mirage unification scale

can slide up or down depending on model parameters for fixed α_m . As we will see, the mirage unification scale plays a crucial role in the phenomenology of DMM models.

The general expressions for the soft supersymmetry breaking terms in deflected mirage mediation have been presented in [8, 9, 16]. However, since we will consider only a particular subset of the possible parameter space, here we will rewrite them in a slightly more transparent form. To start, we first will comment about the model parameters in DMM. The dimensionful parameters include the following:

- A common mass scale M_0 , which sets the overall scale of the soft terms,
- M_{mess} , the messenger scale associated with gauge mediation. This scale can range from the 10 – 100 TeV scale to the GUT scale.

In addition to the usual $\tan\beta$ and sign of μ , the dimensionless parameters include

- α_m , the ratio of anomaly mediation to gravity mediation. The theoretically-motivated range for this parameter is $0 \leq \alpha_m \leq 2$.
- α_g , the ratio of gauge mediation to anomaly mediation. The theoretically-motivated range for this parameter is $-1 \leq \alpha_g \leq 2$, as shown in [9].
- N , the number of messenger pairs. Here the messengers are assumed to be five-plets under a unified $SU(5)$ gauge symmetry that includes the SM gauge group.
- $\{n_i\}$, the so-called modular weights of the MSSM multiplets.

The modular weights, which describe the couplings of the matter fields to the Kähler modulus, can in principle be flavor and generation-dependent. To avoid this issue, we will fix the modular weights to the following standard values (as done also in the phenomenological studies given in [8, 9, 16]): $n_i = 1/2$ for the matter fields and $n_i = 1$ for the Higgs fields.¹ Under these assumptions, and defining the quantity

$$\tilde{\alpha}_m = \alpha_m \left(\frac{1}{16\pi^2} \ln \frac{M_P}{m_{3/2}} \right), \quad (2.1)$$

in which M_P is the Planck mass and $m_{3/2}$ is the gravitino mass, the gaugino masses are

$$M_a(M_G) = M_0[1 + g_0^2(b_a + N)\tilde{\alpha}_m], \quad (2.2)$$

and the threshold corrections are given by $M_a(M_{\text{mess}}^-) = M_a(M_{\text{mess}}^+) + \Delta M_a$, in which

$$\Delta M_a = -NM_0g_a^2(M_{\text{mess}})\tilde{\alpha}_m(1 + \alpha_g). \quad (2.3)$$

In the above, $g_0 = g_a(M_G)$ is the unified gauge coupling at M_G , and b_a are the MSSM beta functions ($b_3 = -3$, $b_2 = 1$, $b_1 = 33/5$). The trilinear couplings for the third generation, which receive no threshold corrections, are given by

$$A_{t,b,\tau}(M_G) = M_0[1 + b_{t,b,\tau}\tilde{\alpha}_m], \quad (2.4)$$

¹For examples in which the modular weights are varied in mirage mediation models, see [12].

in which $b_{t,b,\tau}$ are given by $b_t = 6y_t^2 + y_b^2 - \frac{16}{3}g_3^2 - 3g_2^2 - \frac{13}{15}g_1^2$, $b_b = 6y_b^2 + y_t^2 + y_\tau^2 - \frac{16}{3}g_3^2 - 3g_2^2 - \frac{7}{15}g_1^2$, and $b_\tau = 3y_b^2 + 4y_\tau^2 - 3g_2^2 - \frac{9}{5}g_1^2$, where the third generation Yukawa couplings $y_{t,b,\tau}$ and the gauge couplings are all evaluated at the GUT scale. The soft scalar mass-squared parameters of the matter (denoted by $m_{\tilde{f}_i}^2$) and Higgs fields at the GUT scale are given by

$$\begin{aligned} m_{\tilde{f}_i}^2(M_G) &= M_0^2 \left[\frac{1}{2} - \theta_{\tilde{f}_i} \tilde{\alpha}_m - \dot{\gamma}'_{\tilde{f}_i} \tilde{\alpha}_m^2 \right] \\ m_{H_{u,d}}^2(M_G) &= -M_0^2 \left[\theta_{H_{u,d}} \tilde{\alpha}_m + \dot{\gamma}'_{H_{u,d}} \tilde{\alpha}_m^2 \right], \end{aligned} \quad (2.5)$$

in which $\theta_i = 4 \sum_a g_a^2 c_a^{(i)} - \sum_{i,j,k} |y_{ijk}|^2$ and $\dot{\gamma}'_i = 2 \sum_a g_a^4 (b_a + N) c_a^{(i)} - \sum_{lm} |y_{ilm}|^2 b_{y_{ilm}}$, where $c_a^{(i)}$ are the quadratic Casimirs and y_{ijk} denote the relevant Yukawa couplings. The gauge and Yukawa couplings are again evaluated at M_G . The soft scalar mass-squared parameters also have threshold corrections, $m_i^2(M_{\text{mess}}^-) = m_i^2(M_{\text{mess}}^+) + \Delta m_i^2$, which are

$$\Delta m_i^2 = M_0^2 \sum_a 2c_a^{(i)} N g_a^4(M_{\text{mess}}) \tilde{\alpha}_m (1 + \alpha_g). \quad (2.6)$$

We list these corrections, as well as the $b_{t,b,\tau}$, θ_i , and $\dot{\gamma}'_i$ parameters, in the Appendix.

From Eqs. (2.2), (2.4), and (2.5), we see that when $\alpha_m \rightarrow 0$, the anomaly mediation contributions vanish. The gauge mediation contributions, which enter the threshold corrections of Eqs. (2.3) and (2.6), clearly vanish when the number of messengers $N \rightarrow 0$. If both α_m and N are zero, the theory is thus a modulus/supergravity theory (akin to dilaton domination [18]) that is more restrictive than mSUGRA. More precisely, in this limit the gaugino masses and A terms are unified, the MSSM matter fields have a common scalar mass that is related to the gaugino masses, and the Higgs fields have vanishing soft mass-squares at the GUT scale (*i.e.*, it is a specific subset of non-universal Higgs (NUH) extensions of mSUGRA). Hence, although the DMM framework as considered in this paper has a larger parameter space and hence is a more general framework than mSUGRA, it does not contain mSUGRA as a specific limit.

The threshold corrections that result from integrating out the messenger pairs at M_{mess} have significant effects on the low energy spectrum. For nonzero N , these corrections are governed by α_g . The threshold corrections from gauge mediation and anomaly mediation interfere destructively when $\alpha_g < 0$, with perfect cancellation when $\alpha_g = -1$. Even when $\alpha_g = 0$, the effects of the messengers still are present, as long as $N \neq 0$.

We close this section with a discussion of mirage unification in DMM models, which plays a primary role in governing the superpartner masses. The mirage unification scale in the gaugino sector, which is the scale at which the gauginos appear to unify, is given by

$$M_{\text{mir}} = M_G \left(\frac{m_{3/2}}{M_{Pl}} \right)^{\alpha_m \rho / 2}, \quad (2.7)$$

in which the parameter ρ is

$$\rho = \left(1 + \frac{2N g_0^2}{16\pi^2} \ln \frac{M_{\text{GUT}}}{M_{\text{mess}}} \right) \left(1 - \frac{\alpha_m \alpha_g N g_0^2}{16\pi^2} \ln \frac{M_P}{m_{3/2}} \right)^{-1}. \quad (2.8)$$

In the mirage mediation limit of $N = 0$, the mirage unification scale is at an intermediate scale for the standard KKL T value of $\alpha_m = 1$, and is at the TeV scale for $\alpha_m = 2$. For nonzero N , this scale can be pushed up or down depending on the magnitude and sign of α_g . In general, the lowering of the mirage unification scale from that of the pure supergravity limit of M_G results in a more compressed spectrum in the gaugino sector, such that one expects DMM models to be characterized by distinctive gaugino mass ratios and a greater possibility of mixed-composition lightest neutralinos. In our landscape study that follows, we will see that it will be useful to characterize different possible hierarchy patterns in DMM models according to the mirage unification scale.

3. Methodology and Bounds

To get an adequate survey of the hierarchy patterns in mSUGRA and DMM models, we have generated large sets of model parameters and corresponding low energy spectra, then study how the patterns of the lightest four non-SM particles (superpartners and non-SM Higgs fields) vary as we impose a series of phenomenological bounds. In this section, we will provide a detailed overview of our general procedure and methodology.

The first step is the generation of models. For mSUGRA models, we followed the procedure of FLN [5] and generated 2 million mSUGRA models by randomly selecting input parameters from the following ranges with flat distributions in the parameters:

$$\left\{ \begin{array}{l} 0 \leq m_0 \leq 4 \text{ TeV} \\ 0 \leq m_{1/2} \leq 2 \text{ TeV} \\ \left| \frac{A_0}{m_0} \right| \leq 10 \\ 1 \leq \tan \beta \leq 60 \end{array} \right\}. \quad (3.1)$$

We chose identical ranges to those studied by FLN for purposes of comparison. For the case of DMM models, which involve a larger parameter space and have not been studied in this way in previous literature, we generated a much larger model set consisting of 24.75 million models. The models in this set were obtained by randomly scanning over the DMM parameter ranges given below with flat priors:

$$\left\{ \begin{array}{l} 1 \leq N \leq 5 \\ 4 \leq \log(M_{\text{mess}}/\text{GeV}) \leq 16 \\ 50 \text{ GeV} \leq M_0 \leq 2000 \text{ GeV} \\ 0 \leq \alpha_m \leq 2 \\ -1 \leq \alpha_g \leq 2 \\ 1 \leq \tan \beta \leq 60 \end{array} \right\}. \quad (3.2)$$

As described in the previous section, the ranges chosen for the dimensionless ratio parameters α_m and α_g are the theoretically-motivated ranges studied in previous literature [9, 11]. We scanned the logarithm of the messenger scale $\log(M_{\text{mess}})$ with a uniform distribution between 4 and 16. We also made the specific choice always to include effects of gauge mediation messenger pairs by restricting their number N to take nonzero values.

After generating our model sets for both mSUGRA and DMM, the parameters are then evolved to the electroweak symmetry-breaking scale using `SoftSUSY 3.0.7` with a default low-energy scale of $m_{\text{EW}} = \sqrt{m_{\tilde{t}_1} m_{\tilde{t}_2}}$. For the DMM models, it was necessary to modify `SoftSUSY` to handle the threshold effects, as we did in previous DMM studies [16]. Having obtained the soft supersymmetry breaking parameters at the electroweak scale, we then use `SoftSUSY` and `MicrOmegas` to determine the physical mass spectrum as well as collider and cosmological observables.

At this point we impose a sequence of phenomenological requirements on the candidate models that mirror the requirements imposed in the FLN studies, with updates and modifications where they are needed. The first requirement is the presence of radiative electroweak symmetry-breaking, which in both model sets reduces the sample size by a large fraction. The second requirement is that the lightest R-parity odd state is a neutralino, which we denote as the lightest supersymmetric particle (LSP). We emphasize that the acronym “LSP” refers to this state because, as we will see, quite often the lightest particle beyond those of the Standard Model is one of the heavier Higgs states.

Our third requirement is a series of bounds that we will call the “direct” bounds, in that they reflect conservative direct search limits for new states beyond the Standard Model. These constraints are summarized in Table 1. Many of these constraints are taken directly from FLN [5] and a similar scan by Djouadi *et al.* [19]. However, we have modified and augmented these bounds in several ways. We have augmented the Higgs bounds by including direct limits on the pseudoscalar and charged Higgs masses. In addition, to analyze the effects of tightening the light Higgs mass bound, we employ two separate limits on the Higgs boson mass: the 100 GeV bound of FLN, and the direct limit on the SM Higgs mass of $m_h > 114.4$ GeV. Next, we have added a rather conservative gluino mass bound of $m_{\tilde{g}} \geq 309$ GeV, which arises from the D0 experiment at the Tevatron [20]. This bound is automatically satisfied once the chargino bound is imposed in mSUGRA models; however, this is not necessarily the case in DMM models. Furthermore, it is also necessary to modify not only this bound but also the chargino bound for the case of a squeezed spectrum, which can occur in DMM models. As discussed also in [4], the chargino bound essentially vanishes in the case in which the lightest chargino and the LSP have a high degree of degeneracy ($m_{\tilde{\chi}_1^\pm} - m_{\tilde{\chi}_1^0} < 3$ GeV). Similarly, the gluino bound is degraded when the gauginos are squeezed, as shown in [21, 22]. To model this effect, we employed the (conservative) constraint that the gluino bound degrades to 125 GeV when $m_{\tilde{g}}/m_{\tilde{\chi}_1^0} < 5$.

Our fourth requirement involves indirect constraints on the supersymmetric parameter space arising from the rare decays $b \rightarrow s\gamma$ and $B_s \rightarrow \mu^+\mu^-$, as well as the new physics contributions to the anomalous magnetic moment of the muon. For the inclusive $b \rightarrow s\gamma$ rate, we consider the average value as derived by the Heavy Flavor Averaging Group [23]

$$\text{Br}(b \rightarrow s\gamma) = (355 \pm 24_{-10}^{+9} \pm 3) \times 10^{-6}. \quad (3.3)$$

As shown in Table 2, the range we use is a 3.5σ range about the best fit value:

$$229 \times 10^{-6} \leq \text{Br}(b \rightarrow s\gamma) \leq 481 \times 10^{-6}, \quad (3.4)$$

Condition	Bound
Higgs	$m_h > 100 \text{ GeV}$ or $m_h > 114.4 \text{ GeV}$
Chargino**	$m_{\chi_1^\pm} > 104.5 \text{ GeV}$
Stop	$m_{\tilde{t}_1} > 101.5 \text{ GeV}$
Stau	$m_{\tilde{\tau}_1} > 98.8 \text{ GeV}$
Glauino**	$m_{\tilde{g}} > 309 \text{ GeV}$ ($m_{\tilde{g}} > 125 \text{ GeV}$)
Pseudoscalar Higgs	$m_A > 85 \text{ GeV}$
Charged Higgs	$m_{H^\pm} > 79.3 \text{ GeV}$

Table 1: Direct (collider) mass bounds. Our direct limits follow those of FLN [5], with the following additions. In addition to the FLN Higgs mass limit of 100 GeV, we also consider the SM Higgs mass limit of 114.4 GeV, and include limits on the pseudoscalar and charged Higgs masses. The asterisks indicate that the chargino limit is applied only when the mass difference between the lightest chargino and the LSP exceeds 3 GeV, and the 309 GeV gluino bound is degraded to 125 GeV if the ratio of the gluino mass to the LSP is less than 5, as discussed in the text. For a more detailed analysis of gluino bounds, see [21, 22].

Condition	Bound
$b \rightarrow s\gamma$	$229 \times 10^{-6} \leq \text{Br}(b \rightarrow s\gamma) \leq 481 \times 10^{-6}$
$B_s \rightarrow \mu^+ \mu^-$	$\text{Br}(B_s \rightarrow \mu^+ \mu^-) < 5.8 \times 10^{-8}$
$(g_\mu - 2)_{\text{SUSY}}$	$-11.4 \times 10^{-10} \leq (g_\mu - 2)_{\text{SUSY}} \leq 9.4 \times 10^{-9}$

Table 2: Indirect bounds. Our indirect limits include the update to $\text{Br}(B_s \rightarrow \mu^+ \mu^-)$ rate [24]. We use the HFAG range for $b \rightarrow s\gamma$ [23], and the FLN and Djouadi range for $(g_\mu - 2)_{\text{SUSY}}$.

Condition	Bound
WMAP7	$0.0997 < \Omega_{\tilde{\chi}} h^2 < 0.1221$
WMAP Preferred	$0.07 < \Omega_{\tilde{\chi}} h^2 < 0.14$
WMAP Upper	$\Omega_{\tilde{\chi}} h^2 < 0.121$

Table 3: Dark matter bounds. We consider three options for the dark matter constraints: the WMAP7 2σ range [27], a broader “WMAP Preferred” range, and the WMAP5 upper bound, as used in [4].

which was also used in [7]. We note that the first FLN paper used the slightly tighter range of $283 \times 10^{-6} < \text{Br}(b \rightarrow s\gamma) < 463 \times 10^{-6}$. For the rare decay $B_s \rightarrow \mu^+ \mu^-$, we employ the recent CDF bound [24]:

$$\text{Br}(B_s \rightarrow \mu^+ \mu^-) < 5.8 \times 10^{-8}, \quad (3.5)$$

which is a 95% confidence level upper bound. This bound is significantly more stringent than the one employed in the original papers of FLN, which was $\text{Br}(B_s \rightarrow \mu^+ \mu^-) < 9 \times 10^{-6}$. Finally, for the anomalous magnetic moment of the muon, we constrain the new physics contribution to $g_\mu - 2$ to lie within the conservative range of FLN and Djouadi *et al.*:

$$-11.4 \times 10^{-10} \leq (g_\mu - 2)_{\text{SUSY}} \leq 9.4 \times 10^{-9}. \quad (3.6)$$

Our fifth and final requirement is to impose that the thermal relic density of neutralinos is consistent with the measured cosmological density as inferred from the cosmic microwave background. The standard approach is to assume that the LSP neutralinos make up the entirety of the dark matter. The resulting relic abundance, which is determined by standard cosmology, is then compared to the current constraints from the WMAP satellite to obtain bounds on the SUSY parameter space. The FLN papers used a 2σ bound from WMAP3 of $0.0855 < \Omega_{\tilde{\chi}} h^2 < 0.1189$. WMAP has now reported 1σ results from five years [26] and seven years [27] of observation, as given in Eq. (3.7) and Eq. (3.8), respectively:

$$\Omega_{\tilde{\chi}} h^2|_{5\text{yr}} = 0.1099 \pm 0.0062, \quad (3.7)$$

$$\Omega_{\tilde{\chi}} h^2|_{7\text{yr}} = 0.1109 \pm 0.0056. \quad (3.8)$$

In imposing these bounds, it is important to note that there are caveats to this procedure. The first is that the cosmological assumptions can be questioned: for example, the LSP may not be the only dark candidate, or there may be effects from non-standard cosmology that alter the relic abundance (such as in kination-dominated quintessence theories [28]). Another issue is that the precision quoted in the WMAP results far out-paces that of the theoretical tools available to calculate the value of $\Omega_{\tilde{\chi}} h^2$ from first principles. For our computation we use the package `MicrOmegas 2.2 CPC`, but results from `DarkSUSY` often give values that differ by more than the quoted errors in the WMAP measurements (for example, due to uncertainties in the halo models).

For these reasons, we will consider three options for the dark matter constraints, which are summarized in Table 3. The first is the 2σ range from WMAP7 [27]:

$$0.0997 < \Omega_{\tilde{\chi}} h^2 < 0.1221. \quad (3.9)$$

The second option is to consider a broader range that we call ‘‘WMAP Preferred’’:

$$0.07 \leq \Omega_{\tilde{\chi}} h^2 \leq 0.14, \quad (3.10)$$

which is slightly more expansive than the WMAP3 2σ range utilized by FLN of

$$0.0855 \leq \Omega_{\tilde{\chi}} h^2 \leq 0.121. \quad (3.11)$$

The third option, which is even less restrictive, is to follow the procedure of [4], and only impose an upper limit on the relic abundance obtained from WMAP5:

$$\Omega_{\tilde{\chi}} h^2 \leq 0.121. \quad (3.12)$$

To compare our methodology to that of FLN, it is necessary first to note the difference in treatment of the gaugino mass matrices between `SoftSUSY`, which we employ, and `SuSpect` utilized by FLN. The manner in which radiative corrections are incorporated in `SuSpect` results in an outcome in which the lightest chargino is always lighter than the second-lightest neutralino (when $\mu > 0$). With `SoftSUSY` either mass ordering between these two states is possible, and in fact the ordering can indicate whether the states are primarily wino-like, or whether they have a significant higgsino component. Though typically the

two states are very nearly degenerate in both cases, direct comparisons between our results and those of FLN require some subtlety in grouping outcomes. For this reason, in what follows we will present the hierarchy patterns in mSUGRA with the FLN cuts obtained using `SoftSUSY` as well as the hierarchy patterns of both mSUGRA and DMM with the cuts described in this section, for purposes of comparison.

4. Hierarchy Patterns

4.1 Impact of Progressive Cuts

We now discuss the allowed hierarchy patterns of the lightest four states in minimal supergravity and deflected mirage mediation models. We begin our analysis with a general discussion of the effect of each set of phenomenological requirements on the data sample set for each model. In Table 4, we show the impact of the five progressive cuts described in the previous section, starting with the full data sample of 2 million model points for mSUGRA and 24.75 million model points for DMM. More precisely, we give the number of model points which survive the requirement, beginning with the demand for proper electroweak symmetry breaking. We provide the number of distinct hierarchy patterns which survive, as defined by the absolute ordering of the four lightest new particles. Here we have taken $m_h > 100$ GeV and chosen the WMAP Preferred range of Eq. (3.10).

We see from Table 4 that the combination of gravity, gauge and anomaly mediation in DMM provides a much richer set of possible low-scale outcomes than what occur in mSUGRA, as evidenced by the substantially larger number of hierarchy patterns that emerge at each stage in the cuts. As a result, while the requirement of radiative electroweak symmetry breaking imposes a significant constraint for each data set, it is a more stringent requirement in mSUGRA models (34.3% of the full data sample survives) than in DMM models (71.0% of the full data sample survives). Once this requirement is satisfied, however, the impact of the remaining progressive cuts is similar for the two cases. The indirect limits are slightly more stringent for the DMM models than for mSUGRA models, with $b \rightarrow s\gamma$ and $B_s \rightarrow \mu^+\mu^-$ providing the strongest limits. The $b \rightarrow s\gamma$ bound constrains in particular models with light charginos, which often occur in deflected mirage mediation since the gaugino spectrum is generically squeezed in comparison to that of minimal supergravity. The $B_s \rightarrow \mu^+\mu^-$ constraint tends to reduce the number of scenarios in which the additional Higgs bosons H , A , and H^\pm are light. As we will see, these patterns often occur in DMM, so these limits have a significant effect on the associated model space.

As one might expect, the imposition of the relic density constraint – even a generous one as in Eq. (3.11) – has a dramatic impact on the size of the allowed parameter space and on the nature of the hierarchy patterns that survive. While the dark matter constraints are extremely limiting for both model sets, they are much easier to satisfy in the DMM parameter space than in the mSUGRA parameter space. The reason for this is that there are more possible ways in which the relic abundance constraint can be satisfied in DMM than there are in mSUGRA. It is well known that most of the viable parameter space in mSUGRA results in a bino-like LSP, which typically results in a thermal relic abundance well in excess of the upper bounds in Eq. (3.11) (the exception is the hyperbolic

Requirement	mSUGRA Sample			DMM Sample		
	Points	%	Patterns	Points	%	Patterns
Radiative EWSB	686,204	–	195	17,580,869	–	1338
Neutralino LSP	528,140	77.0%	105	13,639,985	77.6%	380
Direct Search Limits	491,262	71.6%	64	12,332,788	70.1%	226
Indirect Limits	477,608	69.6%	52	9,948,427	56.6%	194
WMAP Preferred Range	3,829	0.6%	35	657,624	3.7%	96

Table 4: Progressive Cuts and Impact on Final Data Sample Size. The number of surviving mSUGRA and DMM models is given as a series of progressive cuts is imposed. The second column of each of the model categories is the percentage of surviving models with respect to the number of models that survives the radiative electroweak symmetry breaking constraint. The light Higgs mass bound is 100 GeV.

NLSP	Proper EWSB		Neutralino LSP		Exper. Bounds		WMAP Preferred	
	# Models	%	# Models	%	# Models	%	# Models	%
χ_2^0	348,859	50.8%	348,849	66.1%	323,167	67.7%	981	25.6%
χ_1^\pm	20,614	3.0%	20,614	3.9%	8,312	1.7%	648	16.9%
$\tilde{\tau}_1$	131,809	19.2%	131,809	25.0%	125,492	26.3%	1,870	48.8%
\tilde{g}	70	0.0%	70	0.0%	0	–	0	–
\tilde{t}_1	16,039	2.3%	16,039	3.0%	12,899	2.7%	227	5.9%
H or A	8,338	1.2%	8,338	1.6%	6,720	1.4%	98	2.6%
$\tilde{\nu}$	63	0.0%	63	0.0%	0	–	0	–
Higgs LSP	2,790	0.4%	2,358	0.4%	1018	0.2%	5	0.1%
$\tilde{\nu}$ LSP	15	0.0%	0	–	0	–	0	–
Other LSP	157,607	23.0%	0	–	0	–	0	–

Table 5: Progressive cuts in mSUGRA. We list the NLSPs of minimal supergravity models as a series of progressive cuts is imposed. The experimental bounds include the direct and indirect bounds in Tables 1 and 2, with $m_h > 100$ GeV.

branch/focus point region, in which the LSP has a nontrivial higgsino component). Co-annihilation channels or resonance effects are thus needed in the early universe to reduce the resulting abundance at freeze-out to acceptable levels, which disproportionately favors models with light staus or stops (see e.g. [1, 2] for reviews). In deflected mirage mediation, we will see that the LSP can be bino-like as in mSUGRA models, but it can also be purely higgsino with an LSP mass in the TeV range, or it can be a mixture of gauginos and higgsinos, *i.e.*, a “well-tempered” neutralino [32].

To see the impact of the cuts on the light states, we now track the nature of the LSP and the NLSP through each stage of the phenomenological requirements, grouping the direct search bounds with the indirect constraints. The results for mSUGRA models are shown in Table 5. We first note that there is a sizable set of patterns in which the lightest chargino is the NLSP; as mentioned previously, this is a result from running `SoftSUSY` as opposed to `SuSpect`, as done in FLN. We see from Table 5 that the direct and indirect constraints affect all NLSP categories more or less equally, but the dark matter requirement heavily favors co-annihilation with staus or stops or (to a lesser extent) charginos. It is notable that there are relatively few models in which the chargino is the NLSP in the

NLSP	Proper EWSB		Neutralino LSP		Exper. Bounds		WMAP Preferred	
	# Models	%	# Models	%	# Models	%	# Models	%
χ_2^0	3,494,589	19.9%	3,494,589	25.6%	3,184,847	32.0%	104,672	15.9%
χ_1^\pm	4,604,411	26.2%	4,604,411	33.8%	2,777,966	27.9%	222,095	33.8%
$\tilde{\tau}_1$	3,271,607	18.6%	3,271,607	24.0%	2,774,387	27.9%	105,472	16.0%
\tilde{g}	16,731	0.1%	16,731	0.1%	7,185	0.1%	0	–
\tilde{t}_1	2,871	0.0%	2,871	0.0%	149	0.0%	7	0.0%
\tilde{e}_R	37,921	0.2%	37,921	0.3%	33,701	0.3%	282	0.0%
H or A	242,500	1.4%	242,500	1.8%	148,322	1.5%	14,676	2.2%
$\tilde{\nu}$	5,653	0.0%	5,653	0.0%	0	–	0	–
Higgs LSP	3,106,146	17.7%	1,963,702	14.4%	1,021,870	10.3%	210,420	32.0%
$\tilde{\nu}$ LSP	4,310	0.0%	0	–	0	–	0	–
Other LSP	2,794,130	15.9%	0	–	0	–	0	–

Table 6: Progressive cuts in DMM. The NLSPs in deflected mirage mediation models are given with the same set of progressive cuts used in the previous table.

original dataset, although such points are relatively more favorable from the dark matter viewpoint. We also see that patterns in which the heavy Higgses are the NLSP or are lighter than the lightest neutralino are quite rare, which is consistent with the FLN results.

In Table 6, we show the same results for DMM models. In contrast with the mSUGRA results, we see that the preferred patterns from the dark matter constraints are the chargino NLSP and Higgs LSP patterns. The stau NLSP patterns are no longer particularly favored, although a significant number of them remain. One reason for this feature is that there are additional avenues in DMM models for obtaining a roughly correct relic density, as mentioned previously. Another reason is that the overall mass scale for the scalars and gauginos are controlled by the same mass scale M_0 in DMM models and it is the gauginos that can be more easily deflected by threshold corrections to lower values. Furthermore, in DMM models the trilinear couplings (A terms) are not separately adjustable, which also affects the low energy spectrum. This is clearly a different situation than the mSUGRA case, where the masses of the scalars and the gauginos are governed by two separately adjustable parameters (m_0 and $m_{1/2}$), and the left-right scalar mixing terms also have contributions from the independent parameter A_0 . For this reason, patterns in which sfermions are the NLSP are relatively disfavored in DMM models. We see this most strikingly in the paucity of stop NLSP patterns. Even before any experimental cuts, the percentage of stop NLSP patterns in the full data set is significantly smaller than it is in mSUGRA, and with the experimental cuts and the dark matter cuts imposed the stop NLSP patterns are completely eliminated. The selectron NLSP patterns, while numerically insignificant, also result from these features. In this very unexpected pattern from the point of view of minimal supergravity, the selectron NLSP is highly degenerate with the stau, and the patterns share similar features with stau NLSP models.

Table 6 also shows that gluino NLSP patterns are also absent in DMM models once the dark matter cuts are imposed. While the absence of gluino NLSPs is expected in mSUGRA, one might think that such patterns might occur in deflected mirage mediation, given the generic possibility of relatively light gluinos [16]. While it is indeed true that

NLSP	WMAP Preferred		WMAP 7-Year		Upper Bound Only	
	mSUGRA	DMM	mSUGRA	DMM	mSUGRA	DMM
χ_2^0	25.6	15.9	26.3	18.3	23.8	5.3
χ_1^\pm	16.9	33.8	15.2	33.9	35.4	62.0
$\tilde{\tau}_1$	48.8	16.0	51.1	18.8	31.7	6.4
\tilde{g}	–	–	–	–	–	0.2
\tilde{t}_1	5.9	–	5.2	–	7.5	–
H or A	2.6	2.2	2.2	2.1	1.6	1.9
Higgs LSP	0.1	32.0	–	26.8	0.1	24.2
Total Models	3,829	657,624	1,256	179,834	9,213	3,637,491
Number of Patterns	35	96	29	80	40	175

Table 7: NLSPs and Number of Models/Patterns for Different Dark Matter Assumptions. The numbers in the upper table are percentages of the total datasets. The Higgs bound is $m_h > 100$ GeV.

NLSP	WMAP Preferred		WMAP 7-Year		Upper Bound Only	
	mSUGRA	DMM	mSUGRA	DMM	mSUGRA	DMM
χ_2^0	29.5	17.8	29.9	20.7	25.7	7.7
χ_1^\pm	21.2	27.7	19.5	27.9	43.7	52.3
$\tilde{\tau}_1$	44.1	14.1	46.1	16.9	26.7	6.9
\tilde{g}	–	–	–	–	–	0.1
\tilde{t}_1	2.0	–	1.9	–	2.2	–
H or A	3.1	2.6	2.6	2.5	1.6	1.8
Higgs LSP	0.2	37.7	–	32.0	0.1	31.2
Total Models	2,908	555,631	959	150,392	7,351	2,355,932
Number of Patterns	27	90	24	76	33	137

Table 8: NLSPs and Number of Models/Patterns for Different Dark Matter Assumptions. The numbers in the upper table are percentages of the total datasets. The Higgs bound is $m_h > 114.4$ GeV.

lighter gluinos are more prevalent in DMM, it is difficult to have the gluino as the NLSP. The reason for this is that while the gaugino sector in DMM models is typically squeezed relative to that of mSUGRA models, it requires a precise conspiracy of parameters to make the gluino lighter than the lightest chargino and the second-lightest neutralino, *i.e.*, a mirage unification scale at very particular (low scale) values. This is not generic in DMM, but it can happen – in fact, prior to the dark matter cuts, it is relatively easier to have a gluino NLSP than a stop NLSP. However, such points in parameter space are severely constrained by the dark matter bounds. As we will see, gluino NLSP patterns typically predict too low of a relic abundance because the LSP is generically a mixed-composition state with a relatively low mass, and hence such patterns are completely eliminated by the WMAP preferred constraint.

We now show the impact of the different dark matter cuts and the light Higgs bounds on the NLSPs in both sets of models. The direct and indirect bounds imposed are as given in Tables 1-2, with $m_h > 100$ GeV in Table 7 and $m_h > 114.4$ GeV in Table 8. The WMAP Preferred and WMAP7 bounds show similar results for both models and both

mSP	Hierarchy				FLN Cuts
	1	2	3	4	mSUGRA
mSP2'	χ_1^0	χ_2^0	χ_1^\pm	H, A	10.9
mSP1'	χ_1^0	χ_2^0	χ_1^\pm	χ_3^0	9.3
mSP3'	χ_1^0	χ_2^0	χ_1^\pm	$\tilde{\tau}_1$	2.8
mSP4' (mSP22)	χ_1^0	χ_2^0	χ_1^\pm	\tilde{g}	1.4
	χ_1^0	χ_2^0	χ_3^0	χ_1^\pm	0.6
	χ_1^0	χ_2^0	H, A	χ_1^\pm	0.1
	χ_1^0	χ_2^0	$\tilde{\tau}_1$	χ_1^\pm	0.1
	χ_1^0	χ_2^0	χ_1^\pm	\tilde{t}_1	0.1
mSP1	χ_1^0	χ_1^\pm	χ_2^0	χ_3^0	17.0
mSP5	χ_1^0	$\tilde{\tau}_1$	$\tilde{\ell}_R$	$\tilde{\nu}_3$	20.1
mSP6'	χ_1^0	$\tilde{\tau}_1$	χ_2^0	χ_1^\pm	19.2
mSP7'	χ_1^0	$\tilde{\tau}_1$	$\tilde{\ell}_R$	χ_2^0	3.8
mSP8	χ_1^0	$\tilde{\tau}_1$	H, A		2.9
mSP7	χ_1^0	$\tilde{\tau}_1$	$\tilde{\ell}_R$	χ_1^\pm	0.4
mSP9	χ_1^0	$\tilde{\tau}_1$	$\tilde{\ell}_R$	H, A	0.3
mSP6	χ_1^0	$\tilde{\tau}_1$	χ_1^\pm	χ_2^0	0.1
	χ_1^0	$\tilde{\tau}_1$	\tilde{t}_1	χ_2^0	0.1
	χ_1^0	$\tilde{\tau}_1$	H, A	χ_2^0	0.1
mSP10	χ_1^0	$\tilde{\tau}_1$	\tilde{t}_1	$\tilde{\ell}_R$	0.1
mSP14	χ_1^0	H, A	H^\pm		3.7
mSP15'	χ_1^0	H, A	χ_2^0		0.3
	χ_1^0	H	χ_2^0	A	0.2
mSP16	χ_1^0	H, A	$\tilde{\tau}_1$		0.2
mSP11'	χ_1^0	\tilde{t}_1	χ_2^0	χ_1^\pm	4.5
mSP12'	χ_1^0	\tilde{t}_1	$\tilde{\tau}_1$	χ_2^0	1.0
mSP13	χ_1^0	\tilde{t}_1	$\tilde{\tau}_1$	$\tilde{\ell}_R$	0.4
	H, A	H^\pm	χ_1^0		0.1
	H, A	χ_1^0	H^\pm		0.1

Table 9: Hierarchy Patterns and Relative Percentages: FLN cuts. The hierarchies of the four lightest non-SM states for mSUGRA models with cuts given in FLN [5].

Higgs bounds, with the WMAP7 limits showing a stronger preference for $\tilde{\tau}$ NLSPs than the WMAP Preferred bound, and a weaker preference for Higgs LSP patterns in the DMM case. By comparing Tables 7 and 8, one sees that the effect of the stronger Higgs limit is to lessen the number of stop and stau NLSP cases in minimal supergravity models, and to decrease the number of chargino NLSP cases and increase the number of Higgs LSP cases in deflected mirage mediation models. However, the preference for NLSP patterns is quite different when only the WMAP upper bound is imposed. As expected, for both model sets the number of chargino NLSPs drastically increases and the number of stau NLSPs decreases as compared to what is found with the WMAP Preferred and WMAP7 cuts. Finally, the results show that there are generically many more patterns in DMM models than in mSUGRA models, with the largest number obtained for the allowed DMM patterns satisfying the dark matter upper bound constraint. We will enumerate the details of these hierarchy patterns in the next subsection.

4.2 Hierarchy Patterns in mSUGRA and DMM

We now present the detailed hierarchy patterns of the lightest four non-Standard Model states obtained in minimal supergravity and deflected mirage mediation models. As mentioned, since we used `SoftSUSY` as opposed to `SuSpect` (used by FLN and Berger *et al.*), the details of the hierarchies differ from the FLN results because of the differences of the two codes in handling the chargino and neutralino sectors when the lightest chargino and second-lightest neutralino are nearly degenerate. In this limit, it is found that for minimal supergravity models, the lightest chargino is almost always lighter than the second-lightest neutralino when `SuSpect` is used, while either outcome can occur when `SoftSUSY` is used, depending on whether these two states are wino-dominated or whether they include a nontrivial higgsino component.

To see this more explicitly, we begin by reproducing the mSUGRA analysis of the first FLN paper [5]. The FLN cuts include a 100 GeV Higgs mass bound and direct limits as given in Table 1, the branching ratios $283 \times 10^{-6} < \text{Br}(b \rightarrow s\gamma) < 463 \times 10^{-6}$ and $\text{Br}(B_s \rightarrow \mu^+\mu^-) < 9 \times 10^{-6}$ as well as the muon anomalous magnetic moment limit of Table 2, and the WMAP3 2σ limits, $0.0855 < \Omega_\chi h^2 < 0.1189$. The results are presented in Table 9. We follow the FLN notation in labeling the patterns as mSP1, mSP2, etc., but use primes when the ordering of the lightest chargino and second-lightest neutralino is reversed from that of FLN. We also note that in the FLN papers, the Higgs LSP and Higgs NLSP patterns were grouped together as a single entity, though here we will not do so in anticipation of the DMM results.

Clearly, there are several patterns in which the NLSP is the second-lightest neutralino rather than the lightest chargino. The dominant neutralino NLSP patterns always have the chargino as the third-lightest state, which indicates that the lightest chargino and second-lightest neutralino are wino-like. Such patterns are common in mSUGRA, as the LSP is generically a bino-like state. In fact, the sole surviving chargino NLSP pattern is the mSP1 pattern of FLN, where the second-lightest neutralino is the third-lightest new state. This pattern corresponds to the focus point/hyperbolic branch region of mSUGRA, for which the LSP has a nontrivial higgsino component. We will see that in general, chargino NLSP patterns occur when the LSP composition includes significant higgsino components.

In general, however, the overall percentages obtained from summing the original pattern and the primed pattern (when needed) are in agreement with the FLN results. More precisely, as found in [5], the top five patterns are as follows:

FLN Analysis

- Stau NLSP patterns: (i) $\chi_1^0 < \tilde{\tau}_1 < \tilde{\ell}_R < \tilde{\nu}_3$ (mSP5), and (ii) $\chi_1^0 < \tilde{\tau}_1 < \chi_2^0 < \chi_1^\pm$ (mSP6')
- Chargino NLSP pattern: (iii) $\chi_1^0 < \chi_1^\pm < \chi_2^0 < \chi_3^0$ (mSP1)
- Neutralino NLSP patterns: (iv) $\chi_1^0 < \chi_2^0 < \chi_1^\pm < H, A$ (mSP2'), and (v) $\chi_1^0 < \chi_2^0 < \chi_1^\pm < \chi_3^0$ (mSP1').

As found in FLN, there are also a number of subdominant hierarchy patterns in which the stop is the NLSP, with the most popular one being the $\chi_1^0 < \tilde{t}_1 < \chi_2^0 < \chi_1^\pm$ (mSP11') pattern, and patterns in which the heavy Higgses are the NLSP, with the most popular one being $\chi_1^0 < H, A < H^\pm$ (mSP14).

We now turn to the hierarchy patterns with our updated sets of cuts. The results for both mSUGRA and DMM are presented in Table 10 for $m_h > 100$ GeV, and Table 11 for $m_h > 114.4$ GeV. We include the pattern ordering for all three sets of dark matter bounds in each table, and group mSUGRA and DMM results together for purposes of comparison.

From Tables 10 and 11, we see several general trends in the results. One feature is that the dark matter constraints favor very different patterns for the two models. While in mSUGRA the dominant patterns tend to be stau NLSP patterns, in DMM the favored pattern is always the Higgs LSP pattern, with $H, A < H^\pm < \chi_1^0$. The Higgs LSP pattern found in DMM models is quite different from typical mSUGRA mass patterns, with a relatively squeezed spectrum, an LSP with a mixed composition of bino, wino, and higgsino states, and a high degree of degeneracy between the lightest chargino and the lightest two neutralinos, as we will discuss in greater detail in the next section. The other favored patterns in DMM models generically are those in which the charginos and neutralinos are light compared to the scalar masses, which is expected since the gaugino mass ratios at low energies are adjustable depending on the size of the mirage unification scale and the threshold effects from integrating out the messenger fields from gauge mediation.

Another feature is that for both mSUGRA and DMM models, the WMAP Preferred and WMAP7 bounds result in similar ordering of the most common patterns for a given light Higgs mass limit, but the pattern ordering is quite different for the WMAP upper bound cuts. The WMAP upper bound preferentially selects patterns with light charginos, which include the Higgs LSP pattern and the chargino NLSP patterns. This is as expected, since these patterns typically have LSPs with a significant fraction of wino and/or higgsino components. For all of the dark matter cuts, increasing the bound on the lightest Higgs boson typically disfavors models with lighter scalars, which is also as expected since the Higgs limit tends to require an increase in the third generation scalar masses.

For mSUGRA models with the 100 GeV Higgs mass bound, these two dark matter bounds result in the same top five patterns as the FLN cuts. As expected, increasing the light Higgs mass bound for these two cases then favors the mSUGRA patterns with light charginos, neutralinos, and additional Higgs bosons, and slightly disfavors those light sneutrinos, first/second generation sleptons, and stops. For the 114.4 GeV Higgs bound, the top five patterns for the WMAP preferred and WMAP7 bounds are:

Updated FLN Analysis

- Stau NLSP pattern: (i) $\chi_1^0 < \tilde{\tau}_1 < \chi_2^0 < \chi_1^\pm$ (mSP6')
- Chargino NLSP pattern: (ii) $\chi_1^0 < \chi_1^\pm < \chi_2^0 < \chi_3^0$ (mSP1)
- Stau NLSP pattern: (iii) $\chi_1^0 < \tilde{\tau}_1 < \tilde{\ell}_R < \tilde{\nu}_3$ (mSP5)

Hierarchy					WMAP Preferred		WMAP 7-year		Upper Bound Only	
mSP	1	2	3	4	mSUGRA	DMM	mSUGRA	DMM	mSUGRA	DMM
mSP3'	χ_1^0	χ_2^0	χ_1^\pm	$\tilde{\tau}_1$	3.1	7.1	3.0	8.4	2.1	3.1
mSP2'	χ_1^0	χ_2^0	χ_1^\pm	H, A	10.3	6.8	11.0	7.5	11.4	1.6
mSP4'	χ_1^0	χ_2^0	χ_1^\pm	\tilde{g}	1.8	1.7	1.8	2.0	1.2	0.5
mSP1'	χ_1^0	χ_2^0	χ_1^\pm	\tilde{t}_1	0.1	0.1	0.1	0.1	0.1	–
	χ_1^0	χ_2^0	χ_1^\pm	$\tilde{\ell}_R$	–	0.1	–	0.1	–	–
	χ_1^0	χ_2^0	χ_1^\pm	χ_3^0	9.7	–	9.9	–	8.4	–
	χ_1^0	χ_2^0	χ_3^0	χ_1^\pm	0.6	–	0.3	–	0.6	–
	χ_1^0	χ_1^\pm	χ_2^0	$\tilde{\tau}_1$	0.3	12.6	0.1	14.2	–	22.9
mSP1	χ_1^0	χ_1^\pm	χ_2^0	H, A	0.1	10.8	–	9.3	0.1	9.8
	χ_1^0	χ_1^\pm	χ_2^0	\tilde{g}	–	3.8	–	3.6	–	12.9
	χ_1^0	χ_1^\pm	\tilde{g}	χ_2^0	–	–	–	–	–	4.9
	χ_1^0	χ_1^\pm	H, A	$\tilde{\ell}_R$	–	0.8	–	0.6	–	3.4
	χ_1^0	χ_1^\pm	χ_2^0	$\tilde{\ell}_R$	–	–	–	–	–	1.8
	χ_1^0	χ_1^\pm	χ_2^0	χ_3^0	16.5	3.7	15.0	4	35.2	2.3
	χ_1^0	χ_1^\pm	$\tilde{\ell}_R$	$\tilde{\tau}_1$	–	–	–	–	–	0.6
	χ_1^0	χ_1^\pm	\tilde{g}	H, A	–	–	–	–	–	0.5
	χ_1^0	χ_1^\pm	$\tilde{\tau}_1$	χ_2^0	0.1	0.7	0.1	0.8	–	0.5
	χ_1^0	χ_1^\pm	$\tilde{\tau}_1$	$\tilde{\ell}_R$	–	0.5	–	0.5	–	0.9
	χ_1^0	χ_1^\pm	$\tilde{\ell}_R$	χ_2^0	–	–	–	–	–	0.1
	χ_1^0	χ_1^\pm	χ_2^0	\tilde{t}_1	–	0.8	–	0.9	–	1.0
	χ_1^0	χ_1^\pm	$\tilde{\tau}_1$	H, A	–	0.1	–	0.1	–	0.1
	χ_1^0	χ_1^\pm	H, A	χ_2^0	–	0.1	–	0.1	–	0.2
	mSP6'	χ_1^0	$\tilde{\tau}_1$	χ_2^0	χ_1^\pm	19.7	5.8	21.0	6.7	15.4
mSP7'	χ_1^0	$\tilde{\tau}_1$	$\tilde{\ell}_R$	χ_2^0	4.8	2.7	4.4	3.2	3.7	1.3
mSP8	χ_1^0	$\tilde{\tau}_1$	H, A	χ_1^\pm	1.7	1.6	1.8	1.9	0.8	0.3
mSP7	χ_1^0	$\tilde{\tau}_1$	$\tilde{\ell}_R$	χ_1^\pm	1.3	2.8	1.5	3.3	0.2	1.0
mSP6	χ_1^0	$\tilde{\tau}_1$	χ_1^\pm	χ_2^0	0.5	1.8	0.6	2.2	0.1	0.6
mSP5	χ_1^0	$\tilde{\tau}_1$	χ_1^\pm	$\tilde{\ell}_R$	–	0.7	–	0.7	–	0.4
	χ_1^0	$\tilde{\tau}_1$	$\tilde{\ell}_R$	$\tilde{\nu}$	20.2	0.5	21.0	0.5	11.0	0.1
mSP9	χ_1^0	$\tilde{\tau}_1$	χ_1^\pm	H, A	–	0.1	–	0.2	–	0.1
mSP14	χ_1^0	$\tilde{\tau}_1$	$\tilde{\ell}_R$	H, A	0.2	0.1	0.3	0.1	0.1	–
	χ_1^0	H, A	H^\pm	χ_1^\pm	1.9	1.5	1.8	1.5	1	0.7
mSP15'	χ_1^0	H, A	χ_1^\pm	χ_1^\pm	–	0.4	–	0.3	0.1	1.0
	χ_1^0	H, A	χ_2^0	χ_2^0	0.3	0.2	0.2	0.2	0.4	0.1
mSP16	χ_1^0	H, A	$\tilde{\tau}_1$	$\tilde{\tau}_1$	0.1	0.1	–	0.1	–	–
mSP11'	χ_1^0	\tilde{g}	χ_1^\pm	χ_2^0	–	–	–	–	–	0.2
	χ_1^0	\tilde{t}_1	χ_2^0	χ_1^\pm	4.5	–	4.0	–	5.6	–
	χ_1^0	\tilde{t}_1	$\tilde{\tau}_1$	χ_2^0	0.9	–	0.7	–	1.2	–
mSP12'	χ_1^0	\tilde{t}_1	$\tilde{\tau}_1$	$\tilde{\ell}_R$	0.5	–	0.5	–	0.7	–
	H, A	H^\pm	χ_1^0	H^\pm	0.1	31.3	–	26.2	–	23.0
	H, A	χ_1^0	H^\pm	H^\pm	–	0.6	–	0.5	–	1.0
TOTAL					99.3	99.9	99.1	99.8	99.4	99.6

Table 10: Hierarchy Patterns and Relative Percentages. The hierarchies of the four lightest non-SM states, with some grouping of cases. The Higgs mass bound is $m_h > 100$ GeV.

Hierarchy					WMAP Preferred		WMAP 7-year		Upper Bound Only		
mSP	1	2	3	4	mSUGRA	DMM	mSUGRA	DMM	mSUGRA	DMM	
mSP3'	χ_1^0	χ_2^0	χ_1^\pm	$\tilde{\tau}_1$	2.8	7.9	2.2	9.3	1.8	4.5	
mSP2'	χ_1^0	χ_2^0	χ_1^\pm	H, A	12.0	7.6	13.0	8.7	12.1	2.2	
mSP4'	χ_1^0	χ_2^0	χ_1^\pm	\tilde{g}	1.6	2.0	1.8	2.3	0.9	0.8	
	χ_1^0	χ_2^0	χ_1^\pm	\tilde{t}_1	0.2	0.1	0.1	0.1	–	–	
mSP1'	χ_1^0	χ_2^0	χ_1^\pm	$\tilde{\ell}_R$	–	0.1	–	0.1	–	–	
	χ_1^0	χ_2^0	χ_1^\pm	χ_3^0	12.0	–	12.0	–	10.1	–	
	χ_1^0	χ_2^0	χ_3^0	χ_1^\pm	0.8	–	0.4	–	0.7	–	
	χ_1^0	χ_1^\pm	χ_2^0	$\tilde{\tau}_1$	–	6.7	–	7.8	–	19.3	
mSP1	χ_1^0	χ_1^\pm	χ_2^0	H, A	–	11.7	–	10.5	0.1	10.4	
	χ_1^0	χ_1^\pm	χ_2^0	\tilde{g}	–	3.5	–	3.3	–	10.2	
	χ_1^0	χ_1^\pm	\tilde{g}	χ_2^0	–	–	–	–	–	3.0	
	χ_1^0	χ_1^\pm	H, A	$\tilde{\ell}_R$	–	0.9	–	0.7	–	2.6	
	χ_1^0	χ_1^\pm	χ_2^0	$\tilde{\ell}_R$	–	–	–	–	–	2.5	
	χ_1^0	χ_1^\pm	χ_2^0	χ_3^0	21.0	3.8	20.0	4.3	43.7	2.4	
	χ_1^0	χ_1^\pm	$\tilde{\ell}_R$	$\tilde{\tau}_1$	–	–	–	–	–	0.7	
	χ_1^0	χ_1^\pm	\tilde{g}	H, A	–	–	–	–	–	0.3	
	χ_1^0	χ_1^\pm	$\tilde{\tau}_1$	χ_2^0	–	0.6	–	0.7	–	0.3	
	χ_1^0	χ_1^\pm	$\tilde{\tau}_1$	$\tilde{\ell}_R$	–	0.3	–	0.3	–	0.2	
	χ_1^0	χ_1^\pm	$\tilde{\ell}_R$	χ_2^0	–	–	–	–	–	0.1	
	χ_1^0	χ_1^\pm	χ_2^0	\tilde{t}_1	–	0.1	–	0.2	–	0.1	
	χ_1^0	χ_1^\pm	$\tilde{\tau}_1$	H, A	–	0.1	–	–	–	0.1	
	χ_1^0	χ_1^\pm	H, A	χ_2^0	–	0.1	–	–	–	0.1	
	mSP6'	χ_1^0	$\tilde{\tau}_1$	χ_2^0	χ_1^\pm	23.0	6.7	23.0	7.8	16.0	3.9
	mSP7'	χ_1^0	$\tilde{\tau}_1$	$\tilde{\ell}_R$	χ_2^0	5.3	3.0	4.8	3.5	3.9	1.8
mSP8	χ_1^0	$\tilde{\tau}_1$	H, A	χ_1^\pm	1.9	1.8	2.2	2.4	0.8	0.4	
mSP7	χ_1^0	$\tilde{\tau}_1$	$\tilde{\ell}_R$	χ_1^\pm	–	0.9	–	1.2	–	0.2	
mSP6	χ_1^0	$\tilde{\tau}_1$	χ_1^\pm	χ_2^0	–	0.6	–	0.8	–	0.2	
mSP5	χ_1^0	$\tilde{\tau}_1$	χ_1^\pm	$\tilde{\ell}_R$	–	0.6	–	0.6	–	0.2	
	χ_1^0	$\tilde{\tau}_1$	$\tilde{\ell}_R$	$\tilde{\nu}$	14.0	0.3	15.0	0.3	5.7	0.1	
mSP9	χ_1^0	$\tilde{\tau}_1$	χ_1^\pm	H, A	–	0.2	–	0.2	–	0.1	
	χ_1^0	$\tilde{\tau}_1$	$\tilde{\ell}_R$	H, A	0.3	0.1	0.4	0.1	0.1	–	
mSP14	χ_1^0	H, A	H^\pm	χ_1^\pm	2.2	1.8	2.1	1.7	1.0	1.0	
	χ_1^0	H, A	χ_1^\pm	χ_2^0	–	0.4	0.2	0.3	–	0.7	
mSP15'	χ_1^0	H, A	χ_2^0	χ_1^\pm	0.4	0.2	0.2	0.2	0.5	0.1	
mSP16	χ_1^0	H, A	$\tilde{\tau}_1$	χ_1^\pm	–	0.1	0.1	0.1	–	–	
mSP11'	χ_1^0	\tilde{g}	χ_1^\pm	χ_2^0	–	–	–	–	–	0.1	
	χ_1^0	\tilde{t}_1	χ_2^0	χ_1^\pm	1.7	–	1.8	–	2.0	–	
	χ_1^0	\tilde{t}_1	$\tilde{\tau}_1$	χ_2^0	0.2	–	0.1	–	0.2	–	
mSP12'	χ_1^0	\tilde{t}_1	$\tilde{\tau}_1$	$\tilde{\ell}_R$	–	–	–	–	–	–	
	H, A	H^\pm	χ_1^0	H^\pm	0.2	36.9	–	31.3	0.1	30.3	
	H, A	χ_1^0	H^\pm	H^\pm	–	0.7	–	0.6	–	0.8	
TOTAL					99.6	99.8	99.4	99.4	99.7	99.7	

Table 11: Hierarchy Patterns and Relative Percentages. The hierarchies of the four lightest non-SM states, with some grouping of cases. The Higgs mass bound is $m_h > 114.4$ GeV.

- Neutralino NLSP patterns: (iv) $\chi_1^0 < \chi_2^0 < \chi_1^\pm < H, A$ (mSP2'), and (v) $\chi_1^0 < \chi_2^0 < \chi_1^\pm < \chi_3^0$ (mSP1').

The top five patterns are thus the same as in FLN, but with a slightly different ordering in which the models with light sleptons tend to be less dominant, as seen by the mSP5 pattern dropping from the first to the third most popular pattern.

For DMM models, the dominant hierarchy patterns are different from the FLN set. As seen in Table 10, the WMAP Preferred and WMAP7 dark matter bounds with the 100 GeV Higgs mass bound result in the following top six preferred hierarchy patterns:

DMM Hierarchies: Weak Higgs Bound

- Higgs LSP patterns: (i) $H, A < H^\pm < \chi_1^0$
- Chargino NLSP patterns: (ii) $\chi_1^0 < \chi_1^\pm < \chi_2^0 < \tilde{\tau}_1$ (mSP3), (iii) $\chi_1^0 < \chi_1^\pm < \chi_2^0 < H, A$ (mSP2)
- Neutralino NLSP patterns: (iv) $\chi_1^0 < \chi_2^0 < \chi_1^\pm < \tilde{\tau}_1$ (mSP3'), (v) $\chi_1^0 < \chi_2^0 < \chi_1^\pm < H, A$ (mSP2')
- Stau NLSP pattern: (vi) $\chi_1^0 < \tilde{\tau}_1 < \chi_2^0 < \chi_1^\pm$ (mSP6').

As we have seen, the Higgs LSP pattern, which is negligible in minimal supergravity models (the closest mSUGRA pattern is the Higgs NSLP pattern, mSP14), is the most popular pattern in DMM models. This also holds true for the WMAP upper bound constraint, as well as increasing the light Higgs mass bound. More precisely, from Table 11 we see that for the 114.4 GeV Higgs bound, the top six patterns for the WMAP Preferred and WMAP7 bounds are identical, except that the ordering changes as follows:

DMM Hierarchies: Strict Higgs Bound

- Higgs LSP patterns: (i) $H, A < H^\pm < \chi_1^0$
- Chargino NLSP pattern: (ii) $\chi_1^0 < \chi_1^\pm < \chi_2^0 < H, A$ (mSP2)
- Neutralino NLSP patterns: (iii) $\chi_1^0 < \chi_2^0 < \chi_1^\pm < \tilde{\tau}_1$ (mSP3') and (iv) $\chi_1^0 < \chi_2^0 < \chi_1^\pm < H, A$ (mSP2')
- Chargino NLSP pattern (v) $\chi_1^0 < \chi_1^\pm < \chi_2^0 < \tilde{\tau}_1$ (mSP3) and stau NLSP pattern $\chi_1^0 < \tilde{\tau}_1 < \chi_2^0 < \chi_1^\pm$ (mSP6').

The increased Higgs mass bound has a negligible effect on the Higgs LSP pattern, but it does alter the number of allowed models for each of the other patterns. The most significant effect is for the mSP3 pattern, for which 55% of the viable model points with the 100 GeV Higgs mass bound are lost. The bound also most prominently affects patterns in which the heavy CP odd Higgs boson A is in the lightest four non-SM particles, with 26% of the mSP2 patterns and 17% of the mSP2' patterns with A as the fourth-lightest state lost (as

opposed to the mSP2 and mSP2' patterns with H as the fourth-lightest state, for which 2.6% and 0.03% of the points are lost, respectively).

We see that the top six DMM hierarchy patterns have no overlap with the top five mSUGRA patterns, and that there are also two sets of patterns in which the only difference in the lightest four non-SM particles is the ordering of the lightest chargino and the second-lightest neutralino. It turns out that this ordering is quite important for the phenomenology of DMM models with these patterns. To make this more precise, in what follows we will study the characteristic features of these top six hierarchy patterns for deflected mirage mediation models, focusing on the correlation of specific patterns with the parameter space and general features of the superpartner and Higgs spectra within each pattern.

4.3 DMM Hierarchy Patterns: Parameter Space and Mass Spectra

In this section, we will investigate further details of the DMM top six hierarchy patterns, first focusing on the preferred DMM parameter space for each pattern, and then describing several characteristic features of the typical mass spectra for each pattern. We will discuss each of the top six patterns obtained using the WMAP Preferred constraint on the relic abundance and the light Higgs mass bound of $m_h > 114.4$ GeV, and comment occasionally on the differences that arise when the weaker Higgs mass bound is used. For purposes of presentation, we will group patterns with the same states as the lightest four non-SM particles, such as the DMM mSP2, mSP2' and mSP3, mSP3' patterns.

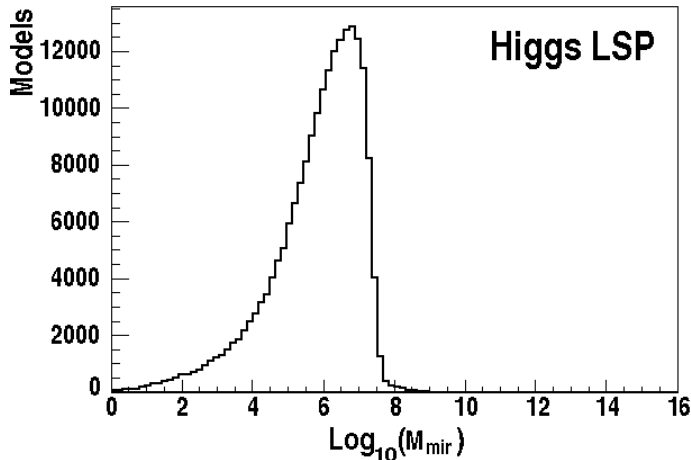


Figure 1: Higgs LSP pattern: mirage unification scale. One-dimensional histogram of the gaugino sector mirage unification scale (in units of GeV) for the Higgs LSP pattern, with the WMAP Preferred dark matter constraints and $m_h > 114.4$ GeV.

- **Higgs LSP ($H, A < H^\pm < \chi_1^0$) pattern.** We begin our analysis with the Higgs LSP hierarchy pattern, which is by far the most dominant pattern in deflected mirage mediation models once the dark matter constraints are included. The first issue we address is to describe the regions of parameter space that give rise to this pattern. To this end, we start by considering the distribution of models in terms of the gaugino sector mirage unification

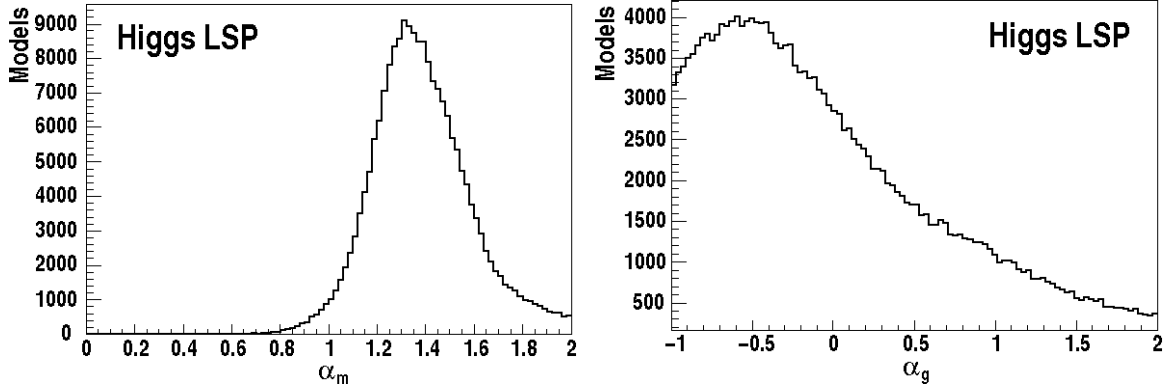


Figure 2: Higgs LSP pattern: α_m and α_g distributions. One-dimensional histograms of α_m (left panel) and α_g (right panel) for the Higgs LSP pattern, with the WMAP Preferred dark matter constraints and $m_h > 114.4$ GeV.

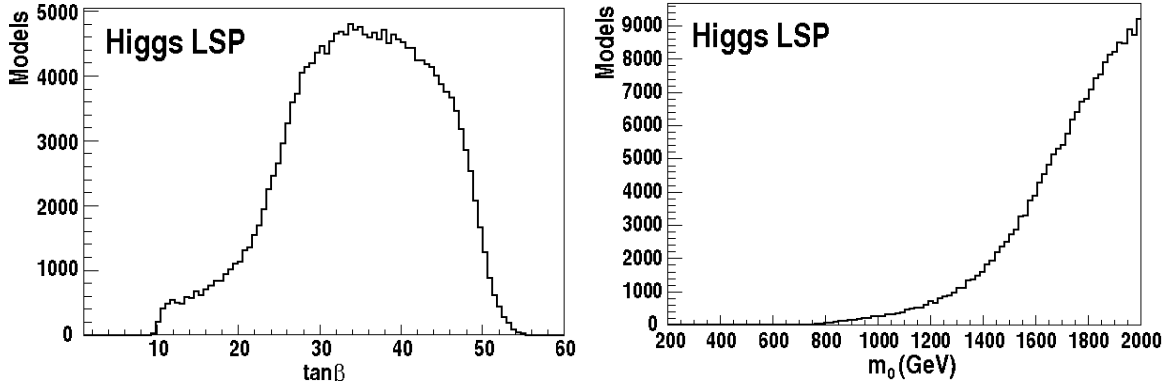


Figure 3: Higgs LSP pattern: $\tan\beta$ and m_0 distributions. One-dimensional histograms of $\tan\beta$ (left panel) and m_0 (right panel) for the Higgs LSP pattern, with the WMAP Preferred dark matter constraints and $m_h > 114.4$ GeV.

scale M_{mir} as given in Eq. (2.7), which we show for the Higgs LSP pattern in Fig. 1. This scale largely dictates the ratio of the gaugino masses at low energies, which has a significant impact on the LSP composition and the resulting relic abundance [33]. Fig. 1 shows that the mirage unification scale is peaked at relatively low values, with a median value of $\sim 10^6$ GeV and a sharp cutoff at 10^8 GeV. As we will see in what follows, this range is characteristic of several of the top six DMM patterns under consideration, and is correlated strongly with the imposition of the dark matter constraints.

Some further structure can be seen by inspecting the corresponding distributions of α_m and α_g , as shown in Fig. 2. For this pattern, the preferred values of α_m are larger than the KKLT value of $\alpha_m = 1$, which indicates that the anomaly mediation contributions are increased with respect to the standard mirage mediation scenario. In addition, though the α_g range is quite broad, it is peaked at negative values, which indicate relatively small threshold corrections associated with gauge mediation. The relatively constrained range

of α_m as opposed to α_g can be understood from the fact that α_m enters the exponent of Eq. (2.7) directly as well as through Eq. (2.8), while α_g enters the exponent only through Eq. (2.8). We will also see this feature in the other hierarchy patterns, and hence we will focus primarily on the α_m distribution in what follows. In terms of the other input parameters, the Higgs LSP pattern also prefers relatively large values of $\tan\beta$ and m_0 , as shown in the two panels of Fig. 3. As we will see momentarily, the typically large values of m_0 result in model spectra with heavier sparticles, with the LSP mass of the order of the TeV scale. The Higgs LSP pattern occurs for all values of the number of messenger pairs N and a broad range of values for the messenger scale M_{mess} , but tends to favor lower values of N and thus smaller thresholds, as well as values of the messenger scale above 10^{10} GeV.

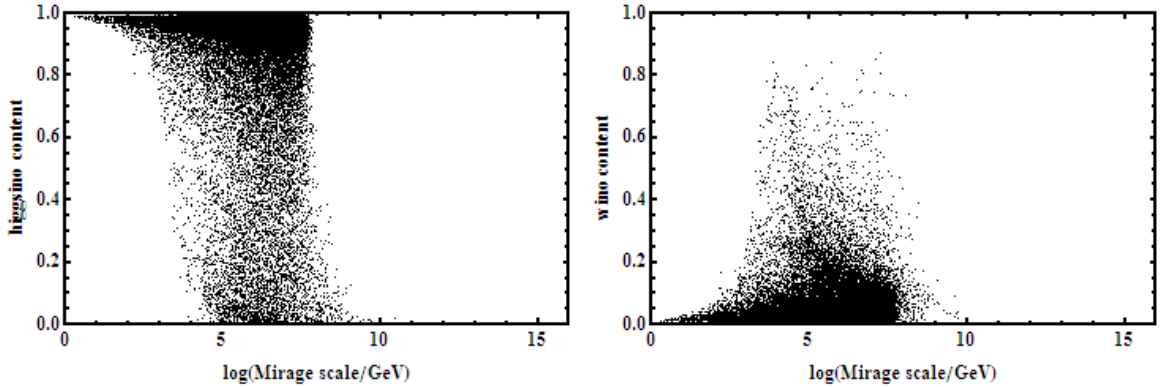


Figure 4: Higgs LSP pattern: higgsino and wino content of χ_1^0 . We plot the higgsino content (left panel) and wino content (right panel) of the lightest neutralino as a function of the mirage unification scale for the Higgs LSP pattern, with the WMAP Preferred dark matter constraints and $m_h > 114.4$ GeV.

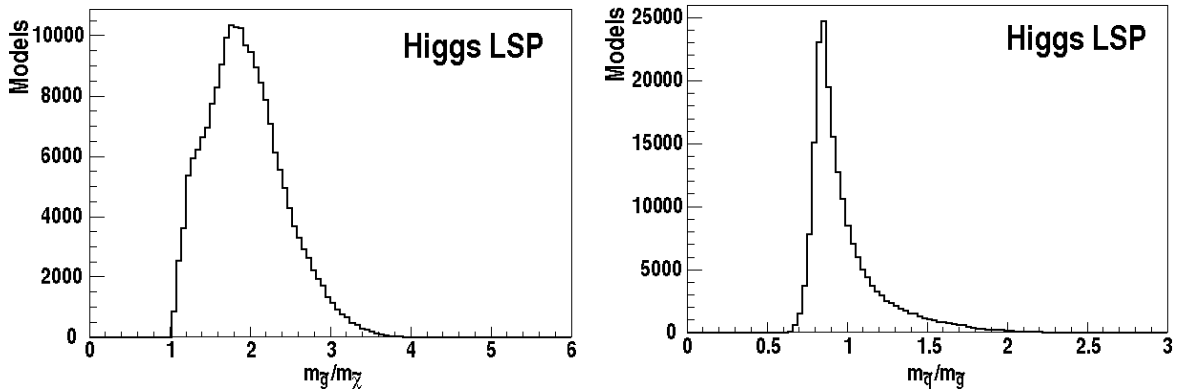


Figure 5: Higgs LSP pattern: $m_{\tilde{g}}/m_{\chi_1^0}$ and $m_{\tilde{q}}/m_{\tilde{g}}$ distributions. Histograms of the ratio of the gluino mass to the lightest neutralino mass (left panel) and the ratio of the first generation squark mass to the gluino mass (right panel) for the Higgs LSP pattern with the WMAP Preferred dark matter constraints and $m_h > 114.4$ GeV.

The mass spectra of the superpartners and Higgs bosons in the Higgs LSP pattern have a number of characteristic features. The lightest neutralino is an example of a well-tempered neutralino, with admixtures of bino, wino, and higgsino components. To see this explicitly, we show in Fig. 4 two-dimensional histograms of the higgsino (left panel) and wino (right panel) fractions of the lightest neutralino as a function of the mirage unification scale. The mass of the lightest neutralino is typically of the order of the TeV scale, and it is very close in mass to the lightest chargino and the next-lightest neutralino, with $(m_{\chi_1^\pm} - m_{\chi_1^0})/m_{\chi_1^0} \sim 0.01$ and $(m_{\chi_2^0} - m_{\chi_1^0})/m_{\chi_1^0} \sim 0.02$ on the average. The gluino is often the heaviest superpartner, and the spectra are generally compressed with respect to typical spectra in minimal supergravity models. In Fig. 5, we show the ratio of the gluino mass to the mass of the lightest superpartner in the left panel, and the ratio of the first generation up-type squark mass to the gluino mass in the right panel. Note that the peak value of the gluino to neutralino mass ratio is about 2, as opposed to the much higher values found in mSUGRA because of the characteristic splitting of the low energy values of the three gaugino masses in minimal supergravity ($M_1 : M_2 : M_3 \sim 1 : 2 : 6$). The first generation squark to gluino mass ratio distribution shows that the gluino and squarks are typically comparable in size, with a slight preference for the gluino to be somewhat heavier than the squarks, such that the gluino is the heaviest colored superpartner. Overall, the spectrum is thus relatively heavy due to the need for a TeV-scale χ_1^0 , but quite compressed. This feature also helps to ensure that the light Higgs mass is heavy enough to evade the 114.4 GeV mass bound. Indeed, relaxing the Higgs bound to 100 GeV (but keeping all other constraints) essentially does not change the number of phenomenologically viable models with this pattern, so it is quite robust with respect to this constraint.

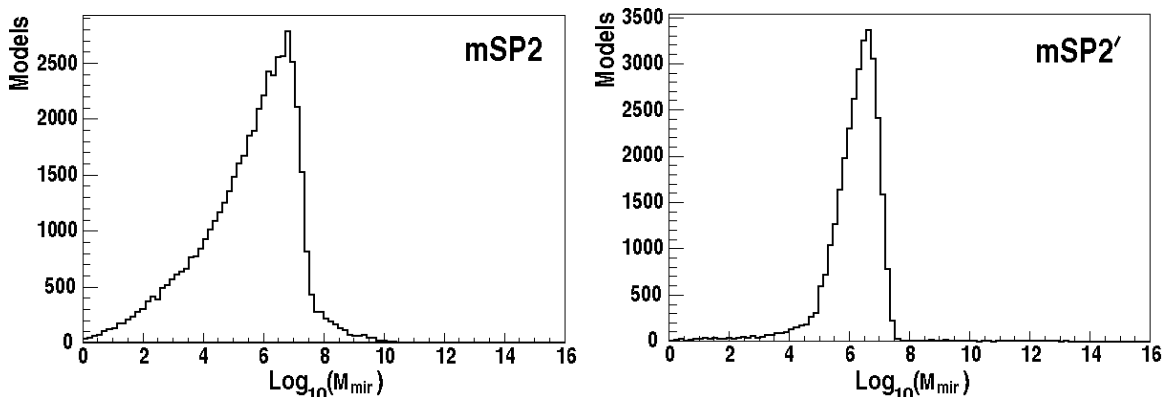


Figure 6: mSP2 and mSP2' patterns: Mirage unification scale. Histograms of the mirage unification scale (in units of GeV) for the mSP2 pattern, $\chi_1^0 < \chi_1^\pm < \chi_2^0 < H, A$ (left panel) and the mSP2' pattern, $\chi_1^0 < \chi_2^0 < \chi_1^\pm < H, A$ (right panel), with the WMAP Preferred dark matter constraints and $m_h > 114.4$ GeV.

• **mSP2** ($\chi_1^0 < \chi_1^\pm < \chi_2^0 < H, A$) and **mSP2'** ($\chi_1^0 < \chi_2^0 < \chi_1^\pm < H, A$) patterns. We now turn to the mSP2 and mSP2' patterns, the two dominant hierarchy patterns in DMM

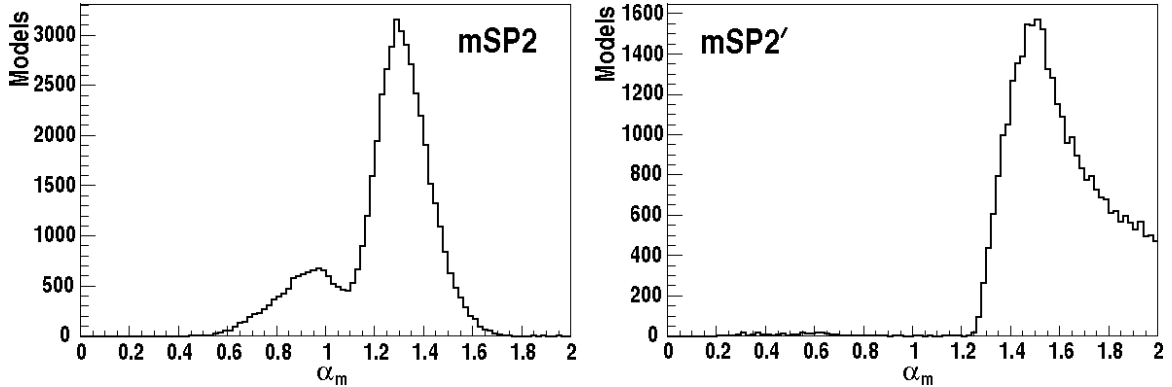


Figure 7: mSP2 and mSP2' patterns: α_m distribution. Histograms of α_m for the mSP2 (left panel) and mSP2' patterns (right panel), with the WMAP Preferred bounds and $m_h > 114.4$ GeV.

models in which the lightest four non-SM particles are the neutralino LSP, the lightest chargino, the second-lightest neutralino, and either the heavy Higgs H or A . In Fig. 6, we show one-dimensional histograms of the mirage unification scale for the mSP2 pattern (left panel) and the mSP2' pattern (right panel). For both patterns, the mirage unification scale peaks at $\sim 10^6$ GeV, with a sharp cutoff at 10^8 GeV, similar to the Higgs LSP pattern. These values are correlated with the distributions of α_m for each pattern, which are shown in Fig. 7. The mSP2 pattern, which has a chargino NLSP, tends to favor values of α_m just above the KKLT value of $\alpha_m = 1$, while the mSP2' pattern, which has a neutralino NLSP, favors larger values of α_m , and hence relatively large contributions from anomaly mediation. For the mSP2 pattern the range of α_g is broad, but mSP2' does exhibit a preference for $\alpha_g \sim -1$, for which the threshold corrections from gauge mediation vanish.

The relatively low values of the mirage unification scale, and in particular the 10^8 GeV cutoff, are associated with the involvement of nontrivial higgsino components in the lightest neutralino. The higgsino composition of the LSP is shown for mSP2 (left panel) and mSP2' (right panel) as a function of the mirage unification scale in Fig. 8. We see that for the mSP2 pattern, the LSP is typically a mixed-composition state that is higgsino-dominated, but for the mSP2' pattern, in the vast majority of cases LSP is purely higgsino. The connection of the LSP composition with the mass ordering of χ_1^\pm and χ_2^0 turns out to be generic for patterns in which the lightest three states are χ_1^0 , χ_1^\pm , and χ_2^0 . We also note that in each pattern, for the few model points that have a mirage unification scale above 10^8 GeV, the LSP no longer has a higgsino component, but rather is a pure bino state. The bino domination of the LSP for models in which the mirage unification scale is large is also a generic feature both in deflected mirage mediation and in mirage mediation, for which the standard KKLT value of $\alpha_m = 1$ results in a mirage unification scale of 10^{10} GeV and a bino-dominated LSP. This connection is expected since the splitting of the gaugino masses increases as the mirage unification scale increases, with the maximal value occurring in the mSUGRA limit in which the mirage scale is of the order of the unification scale.

Turning to the other input parameters, we note that the mSP2 and mSP2' patterns

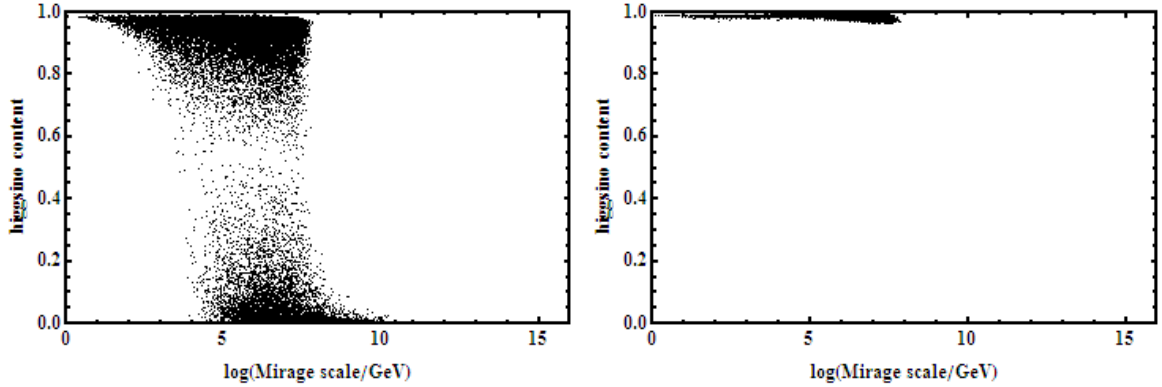


Figure 8: mSP2 and mSP2' patterns: LSP higgsino fraction. Two-dimensional histograms of the higgsino fraction of the neutralino LSP as a function of the mirage unification scale for the mSP2 pattern, $\chi_1^0 < \chi_1^\pm < \chi_2^0 < H, A$ (left panel) and the mSP2' pattern, $\chi_1^0 < \chi_2^0 < \chi_1^\pm < H, A$. The bounds imposed are WMAP Preferred dark matter constraints and $m_h > 114.4$ GeV.

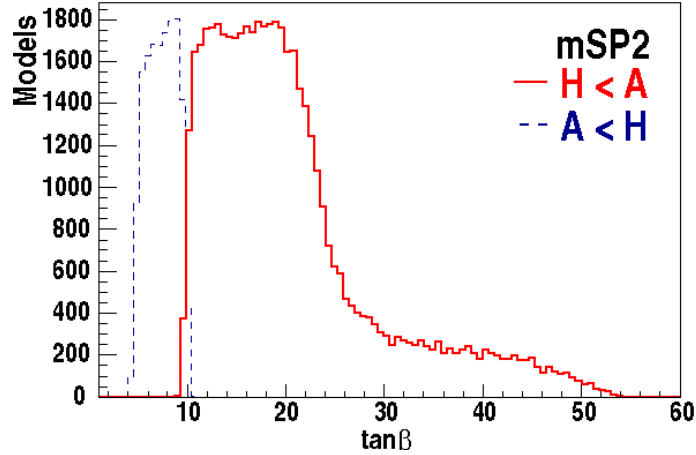


Figure 9: mSP2 pattern: $\tan \beta$ distribution. Histograms of $\tan \beta$ for the mSP2 pattern with $\chi_1^0 < \chi_1^\pm < \chi_2^0 < H, A$, using the WMAP Preferred bounds and $m_h > 114.4$ GeV. The mSP2' pattern (not shown) has similar features, except that the $\chi_1^0 < \chi_2^0 < \chi_1^\pm < H$ distribution is cut off more sharply at $\tan \beta \geq 30$.

both favor lower values of $\tan \beta$ than the Higgs LSP pattern. In Fig. 9, we show the $\tan \beta$ distribution for the mSP2 pattern for the subsets $H < A$ (solid line) and $A < H$ (dashed line) simultaneously. The distribution for mSP2' is similar, with the only significant difference that the larger $\tan \beta$ tail found in the $\chi_1^0 < \chi_1^\pm < \chi_2^0 < H$ distribution is absent for the $\chi_1^0 < \chi_2^0 < \chi_1^\pm < H$ pattern. For both patterns, there is a sharp transition at $\tan \beta = 10$ at which the mass ordering of H and A is reversed; this feature is generic in all of the patterns in which the heavy Higgs bosons are among the lightest four states, and is the reason why patterns with $A < H$ are strongly affected by the light Higgs bound. Both patterns have a broad distribution in M_{mess} and prefer small values of N , as was the case

for the Higgs LSP pattern. The distribution in m_0 is peaked above the TeV range for both patterns, which is expected since the LSP's have significant higgsino fractions in each case.

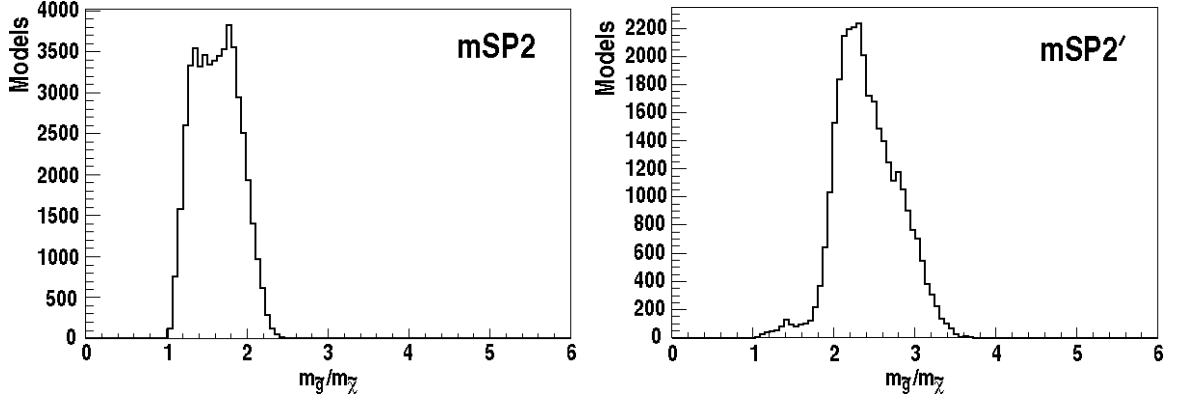


Figure 10: mSP2 and mSP2' patterns: $m_{\tilde{g}}/m_{\chi_1^0}$ distribution. One-dimensional histograms of the ratio of the gluino to LSP mass for the mSP2 pattern (left panel) and mSP2' pattern (right panel), with the WMAP Preferred bounds and $m_h > 114.4$ GeV.

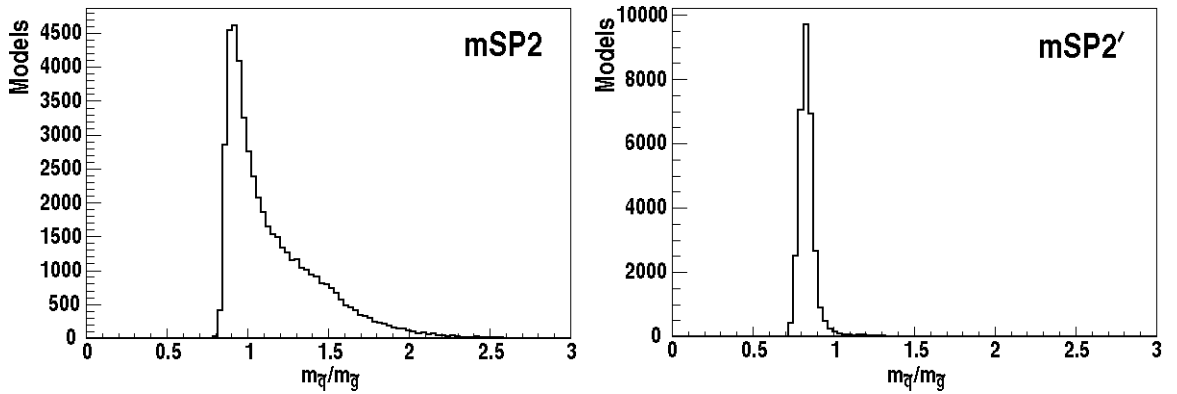


Figure 11: mSP2 and mSP2' patterns: $m_{\tilde{q}}/m_{\tilde{g}}$ distribution. One-dimensional histograms of the ratio of the first generation squark masses to the gluino mass for the mSP2 pattern (left panel) and mSP2' pattern (right panel), with the WMAP Preferred bounds and $m_h > 114.4$ GeV.

The spectrum for the mSP2 and mSP2' patterns also resembles that of the Higgs LSP pattern, with a relatively heavy but compressed spectrum. The lightest chargino and second-lightest neutralino are both highly degenerate with the lightest neutralino: for the mSP2 pattern, on average $(m_{\chi_1^\pm} - m_{\chi_1^0})/m_{\chi_1^0} \sim 0.02$ and $(m_{\chi_2^0} - m_{\chi_1^0})/m_{\chi_1^0} \sim 0.03$, while for mSP2', both $(m_{\chi_1^\pm} - m_{\chi_1^0})/m_{\chi_1^0}$ and $(m_{\chi_2^0} - m_{\chi_1^0})/m_{\chi_1^0} \sim 0.01$. The ratio of the gluino mass to the LSP mass, which is shown in Fig. 10, for mSP2 (left panel) and mSP2' (right panel), shows that the distribution for the mSP2 pattern is peaked at lower values than that of the mSP2' pattern, though both values are still significantly lower than the typical range found in mSUGRA models. The smaller value of this ratio is a generic feature of

chargino NLSP as opposed to neutralino NLSP patterns. The ratio of the first generation squark masses to the gluino mass, which is shown in Fig. 11 for mSP2 (left panel) and mSP2' (right panel), is peaked for both patterns at ratios that are of order one. However, the gluino is generically heavier than the squarks for mSP2', while for mSP2, the gluino can be lighter than the squarks, and possibly the lightest color-charged superpartner.

• **mSP3** ($\chi_1^0 < \chi_1^\pm < \chi_2^0 < \tilde{\tau}$) and **mSP3'** ($\chi_1^0 < \chi_2^0 < \chi_1^\pm < \tilde{\tau}$) patterns. The next patterns we consider are patterns in which the lightest four non-SM particles are the neutralino LSP, the lightest chargino, the second-lightest neutralino, and the lightest stau. We begin with the the mSP3 and mSP3' patterns, in which the the stau is the heaviest of these four states, and either the lightest chargino (mSP3) or the second-lightest neutralino (mSP3') is the NLSP. In Fig. 12, we show one-dimensional histograms of the mirage unification scale for mSP3 (left panel) and mSP3' (right panel), which show a marked difference between the two patterns. For the mSP3 pattern, the mirage unification scale is sharply peaked at $\sim 10^7$ GeV and exhibits the sharp cutoff at $\sim 10^8$ GeV, while the SP3' pattern exhibits a bimodal distribution with the dominant, broader peak at higher values of $\sim 10^{12}$ GeV, and a secondary sharp peak at $\sim 10^7$ GeV. The α_m distributions shown in Fig. 13 are correlated with the mirage unification behavior, in which small values of α_m correspond to large values of the mirage unification scale, and vice versa. As the mirage unification scale is increased between $10^6 - 10^8$, the mass ordering between χ_1^\pm and χ_2^0 flips in some small range, but beyond 10^8 GeV, the NLSP is predominantly a neutralino.

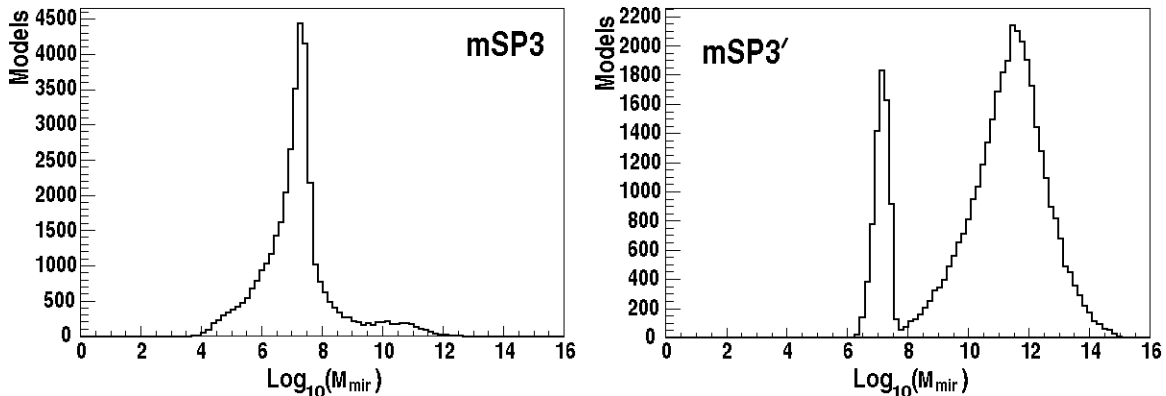


Figure 12: mSP3 and mSP3' patterns: Mirage unification scale. Histograms of the mirage unification scale (in units of GeV) for the mSP3 $\chi_1^0 < \chi_1^\pm < \chi_2^0 < \tilde{\tau}$ (left panel) and the mSP3' patterns, $\chi_1^0 < \chi_2^0 < \chi_1^\pm < \tilde{\tau}$ (right panel), with the WMAP Preferred dark matter constraints and $m_h > 114.4$ GeV.

The mirage unification scale distribution is once again correlated with the detailed composition of the neutralino LSP. In Fig. 14, we show the higgsino composition of the LSP as a function of the mirage unification scale for the mSP3 (left panel) and mSP3' (right panel) patterns. For the chargino NLSP case (mSP3), the lightest neutralino is a mixed-composition state in which the higgsino component often dominates, as was the case

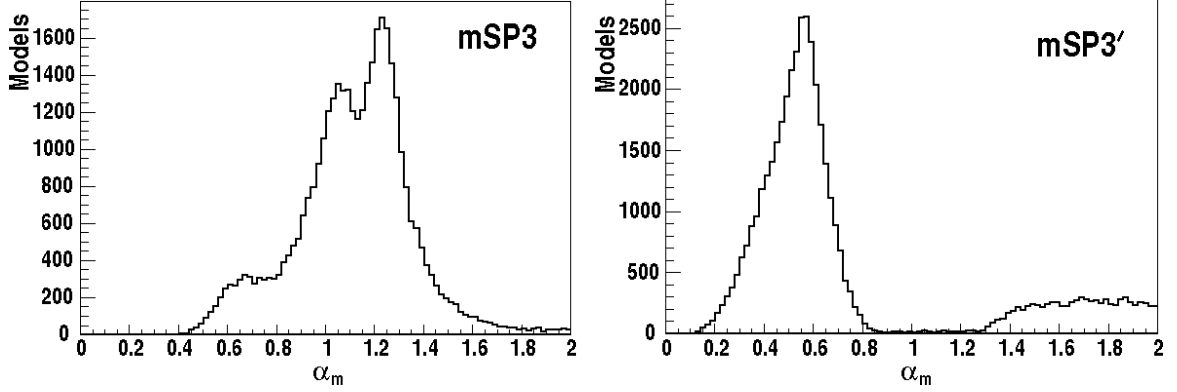


Figure 13: mSP3 and mSP3' patterns: α_m distribution. Histograms of α_m for the mSP3 (left panel) and mSP3' patterns (right panel), with the WMAP Preferred bounds and $m_h > 114.4$ GeV.

for the mSP2 pattern. For the neutralino NLSP pattern (mSP3'), for values of the mirage unification scale below $\sim 10^8$ GeV, the LSP is a pure higgsino state, as was the case for the mSP2' pattern as well. However, for the mSP3' pattern with mirage unification scales above $\sim 10^8$ GeV, the higgsino fraction becomes negligible and the state is pure bino, as in minimal supergravity models.

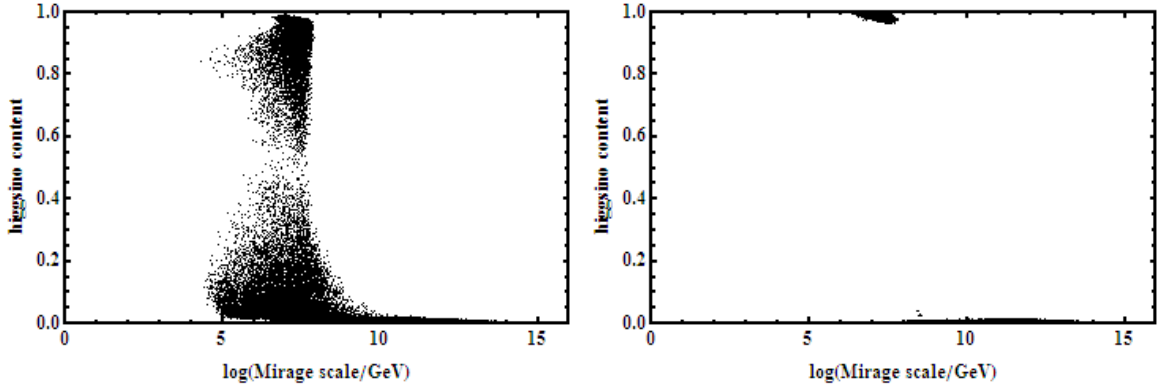


Figure 14: mSP3 and mSP3' patterns: LSP higgsino fraction. Two-dimensional histograms of the LSP higgsino fraction as a function of the mirage unification scale for the mSP3 (left panel) and the mSP3' patterns (right panel), with the WMAP Preferred and $m_h > 114.4$ GeV bounds.

In regards to the other input parameters, the mSP3 pattern favors small values of N , similar to the Higgs LSP pattern. In contrast, the mSP3' pattern has a relatively flat distribution in N . Both patterns have broad distributions in α_g and M_{mess} , but the peak values of each are different for each pattern. For the mSP3 pattern, small negative values of α_g and low values of M_{mess} are favored, while mSP3' prefers values near $\alpha_g = -1$, for which the threshold effects vanish, and high values of M_{mess} . The mSP3 and mSP3' patterns also have broad $\tan\beta$ distributions that peak near low values, as shown in Fig. 15.

The mass spectra for the mSP3 and mSP3' patterns also display the characteristic

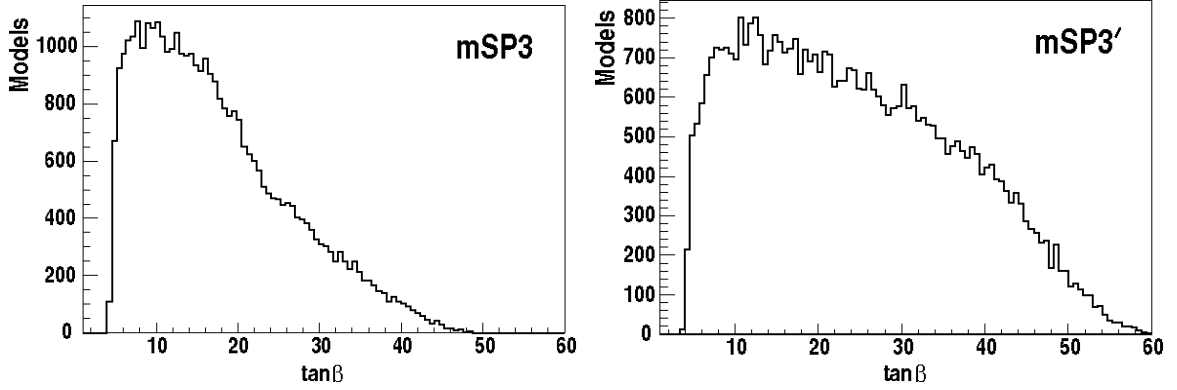


Figure 15: mSP3 and mSP3' patterns: $\tan\beta$ distribution. Histograms of $\tan\beta$ for the mSP3 (left panel) and mSP3' patterns (right panel), using the WMAP Preferred bounds and $m_h > 114.4$ GeV.

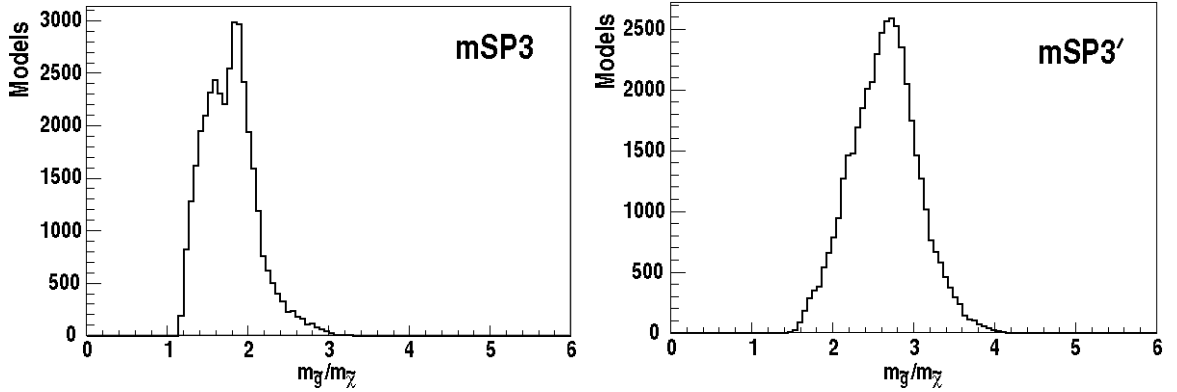


Figure 16: mSP3 and mSP3' patterns: $m_{\tilde{g}}/m_{\chi_1^0}$ distribution. One-dimensional histograms of the ratio of the gluino to LSP mass for the mSP3 (left panel) and mSP3' patterns (right panel), with the WMAP Preferred bounds and $m_h > 114.4$ GeV.

compressed feature of DMM models. In Fig. 16, we show the distribution of $m_{\tilde{g}}/m_{\chi_1^0}$ for the mSP3 pattern (left panel) and the mSP3' pattern (right panel). The results for the mSP3 are similar to those found in the mSP2 pattern of Fig. 10, though the peak is slightly shifted and the tail somewhat extended for the mSP3 pattern. Along the same lines, the mSP2' and mSP3' patterns have similar results that are characteristically larger than those of the mSP2 and mSP3 patterns, though the mSP3' pattern tends to favor slightly larger values. For the ratio of the first generation squark to gluino masses, as shown in Fig. 17 for mSP3 (left panel) and mSP3' (right panel), a comparison with Fig. 11 shows striking similarities with the results for the mSP2 and mSP2' patterns. In particular, the mSP2 and mSP3 distributions of $m_{\tilde{q}}/m_{\tilde{g}}$ are extremely similar. For the mSP3' pattern, the one sharp peak at $m_{\tilde{q}}/m_{\tilde{g}} < 1$ corresponds to the low mirage scale behavior found also in the mSP2' case, but there is also a much larger peak at higher values that corresponds to models with a high mirage unification scale. In the chargino and neutralino sectors, we find

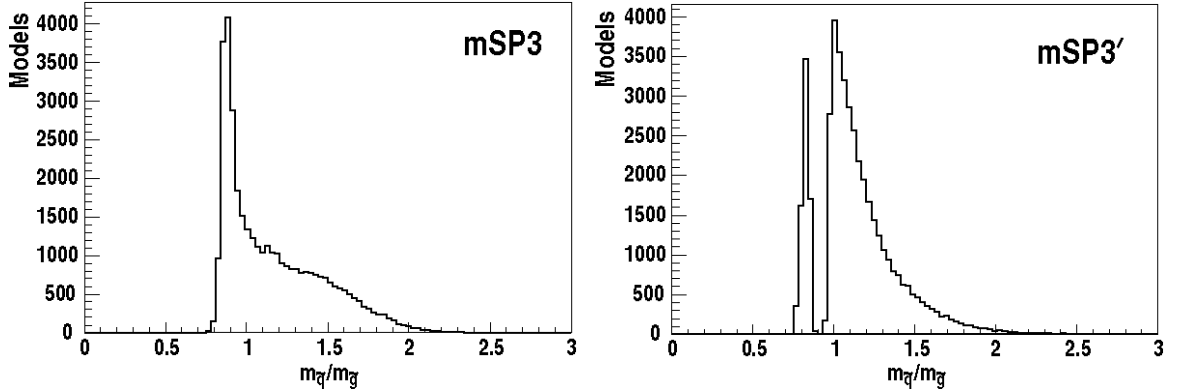


Figure 17: mSP3 and mSP3' patterns: $m_{\tilde{q}}/m_{\tilde{g}}$ distribution. One-dimensional histograms of the ratio of the first generation squark mass to the gluino mass for the mSP3 (left panel) and mSP3' patterns (right panel), with the WMAP Preferred bounds and $m_h > 114.4$ GeV.

that the mass splittings between the LSP and the lightest chargino as well as the second-lightest neutralino are larger for the mSP3 and mSP3' patterns than for the other dominant DMM patterns previously mentioned. More precisely, for the mSP3 pattern, on average $(m_{\chi_1^\pm} - m_{\chi_1^0})/m_{\chi_1^0} \sim 0.05$ and $(m_{\chi_2^0} - m_{\chi_1^0})/m_{\chi_1^0} \sim 0.06$, while for the mSP3' pattern, the splittings are quite significant: both $(m_{\chi_1^\pm} - m_{\chi_1^0})/m_{\chi_1^0}$ and $(m_{\chi_2^0} - m_{\chi_1^0})/m_{\chi_1^0} \sim 0.26$ on average. For the mSP3' pattern, the lightest chargino and the second-lightest neutralino are typically quite degenerate, since for the majority of models there is a bino-like χ_1^0 and a nearly degenerate wino-like pair χ_1^\pm, χ_2^0 , as is often the case in mSUGRA models.

- **mSP6' pattern** ($\chi_1^0 < \tilde{\tau}_1 < \chi_2^0 < \chi_1^\pm$). The final DMM hierarchy pattern that we will consider is the mSP6' pattern, in which the NLSP is the lightest stau. As we will see, this pattern will most strongly resemble typical hierarchy patterns found in minimal supergravity, though the spectrum will once again exhibit the compressed features that are characteristic of DMM models. We begin as usual with the favored input parameter range for the mSP6' pattern, starting with the mirage unification scale, as shown in the left panel of Fig. 18. The mirage unification scale is peaked at high values near $\sim 10^{14}$ GeV, which is near the minimal supergravity limit. This behavior is strongly correlated with the α_m distribution, which is peaked at low values, as seen in the right panel of Fig. 18. The high values of the mirage unification scale correspond to a peaked α_m distribution that favors small α_m values, and thus only small contributions from anomaly mediation as opposed to modulus/gravity mediation. As is the case for most of the DMM patterns, the α_g distribution (not shown) is relatively flat, with no strongly favored regions. The distributions in m_0 shown in the left panel Fig. 19, indicate a preference for significantly lower m_0 values than what has been found in other DMM hierarchy patterns under consideration, which is also correlated with the preference for a high mirage unification scale and the resulting impact on the LSP composition. However, the distributions in N (not shown) and $\tan\beta$, shown in the right panel of Fig. 19, do resemble the previous deflected mirage mediation

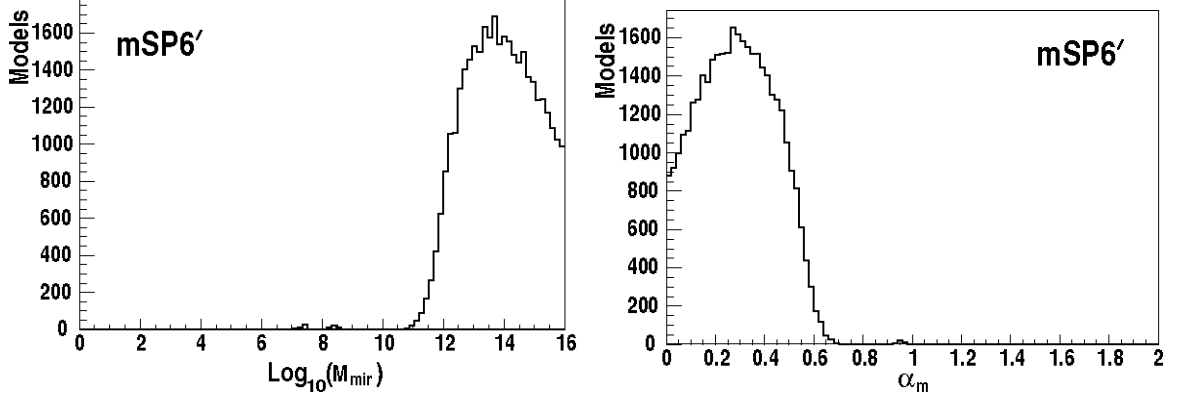


Figure 18: mSP6' pattern: Mirage unification scale and α_m distributions. Histograms of the mirage unification scale (in units of GeV, left panel) and α_m (right panel) for the mSP6' pattern, $\chi_1^0 < \tilde{\tau}_1 < \chi_2^0 < \chi_1^\pm$, with the WMAP Preferred limits and $m_h > 114.4$ GeV.

model patterns, in which there is a preference for low N and larger $\tan\beta$.

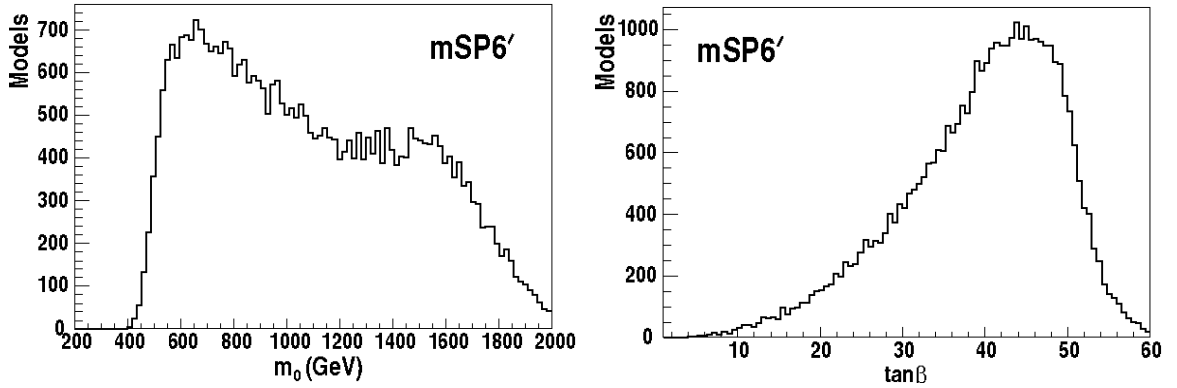


Figure 19: mSP6' pattern: m_0 and $\tan\beta$ distributions. Histograms of m_0 (left panel) and $\tan\beta$ (right panel) for mSP6', with the WMAP Preferred bounds and $m_h > 114.4$ GeV.

The preference for a high mirage unification scale in the mSP6' hierarchy pattern has a direct impact on the composition of the LSP. With the exception of a few isolated model points for which the mirage unification scale is 10^8 GeV or below, the LSP is almost purely a bino state, as in minimal supergravity models. In fact, the mass pattern of the charginos and neutralinos very much resembles that of standard minimal supergravity, with the lowest mass state given by bino-like LSP and the next lightest states in the electroweak chargino/neutralino sector consisting of degenerate wino-like pair consisting of χ_2^0 and χ_1^\pm . The splitting of the χ_1^0 mass compared to the χ_1^\pm and χ_2^0 is more substantial for this pattern, with both $(m_{\chi_1^\pm} - m_{\chi_1^0})/m_{\chi_1^0}$ and $(m_{\chi_2^0} - m_{\chi_1^0})/m_{\chi_1^0} \sim 0.6$ on average.

Due to its many resemblances to minimal supergravity models, the spectrum of the mSP6' pattern is less compressed on the average than the other DMM patterns we have described in this section. In Fig. 20, we plot histograms of the ratio of the gluino mass to the

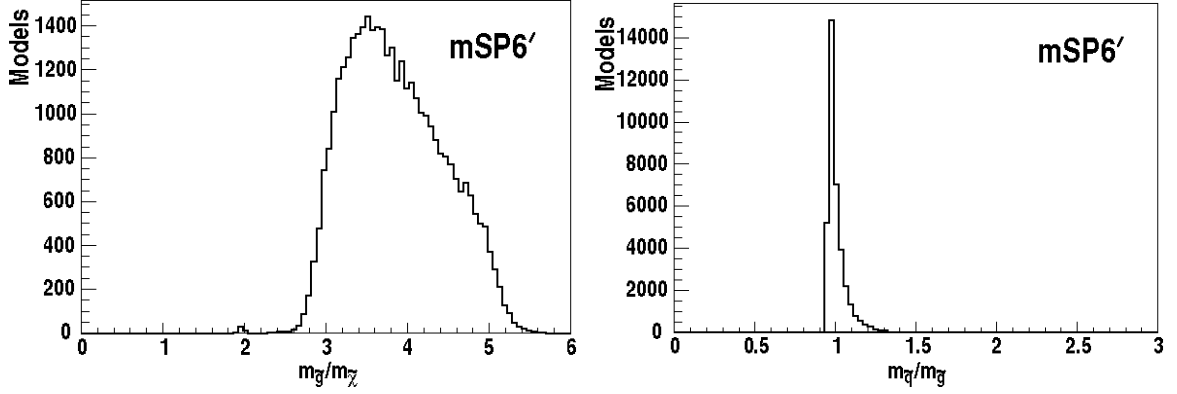


Figure 20: mSP6' pattern: $m_{\tilde{g}}/m_{\chi_1^0}$ and $m_{\tilde{q}}/m_{\tilde{g}}$ distributions. Histograms of the ratio of the gluino mass to the LSP mass (left panel) and the ratio of the first generation squark mass to the gluino mass (right panel) for mSP6', with the WMAP Preferred bounds and $m_h > 114.4$ GeV.

LSP mass (left panel) and the typical first generation squark mass to the gluino mass (right panel). The $m_{\tilde{g}}/m_{\chi_1^0}$ distribution is peaked at significantly larger values than the other DMM patterns, which is as expected since the mSP6' pattern favors high values of the mirage unification scale. For the purposes of comparison, we show in Fig. 21 the gluino to LSP mass ratio for the analogous mSP6' and mSP3' patterns in mSUGRA models, which indicate that this ratio is peaked at still higher values in minimal supergravity. The ratio of the squark to gluino masses in the DMM mSP6' pattern, in contrast, is very sharply peaked at $m_{\tilde{q}}/m_{\tilde{g}} \sim 1$, indicating that on average the first generation squark and gluino masses tend to be quite clustered and significantly heavier than the LSP.

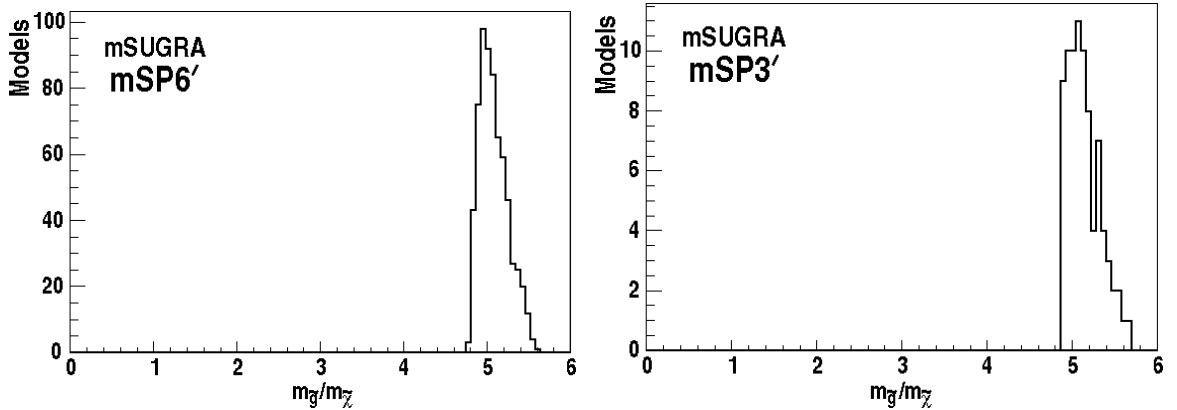


Figure 21: mSUGRA mSP6' and mSP3' patterns: $m_{\tilde{g}}/m_{\chi_1^0}$ distribution. Histograms of the ratio of the gluino mass to the LSP mass in minimal supergravity models for the mSP6' (left panel) and mSP3' (right panel) patterns, with the WMAP Preferred bounds and $m_h > 114.4$ GeV.

5. Summary and Conclusions

In this paper we have taken a bottom-up approach to understanding the phenomenology of deflected mirage mediation, a string-motivated scenario involving comparable contributions to supersymmetry breaking from gravity, anomaly and gauge mediation mechanisms. We have used the hierarchy of mass eigenstates for the superpartners as an organizing principle, and investigated the landscape of these hierarchies for both the mSUGRA and DMM frameworks. Beginning with a substantial data set of input parameters to the DMM model we have applied progressive cuts motivated by phenomenology: radiative electroweak symmetry breaking, a neutral lightest superpartner that can be a dark matter candidate, direct search limits on superpartner masses and indirect limits from rare processes. Of crucial importance was the imposition of thermal relic density constraints for the LSP. Requiring the dark matter candidate to account for all non-baryonic dark matter restricts the parameter set in severe yet interesting ways, while a more relaxed constraint (such as only using the WMAP measurement as an upper bound) allows for a greater variety of model possibilities. Imposing the former (strict) condition we find that there is no overlap between the five most populated hierarchies in mSUGRA with the six most populated hierarchies in deflected mirage mediation. The top six hierarchies account for 77.5% of all DMM models when the WMAP Preferred constraint of (3.10) is imposed. This suggests that a “typical” (phenomenologically allowed) DMM model will look very different from a “typical” model in minimal supergravity.

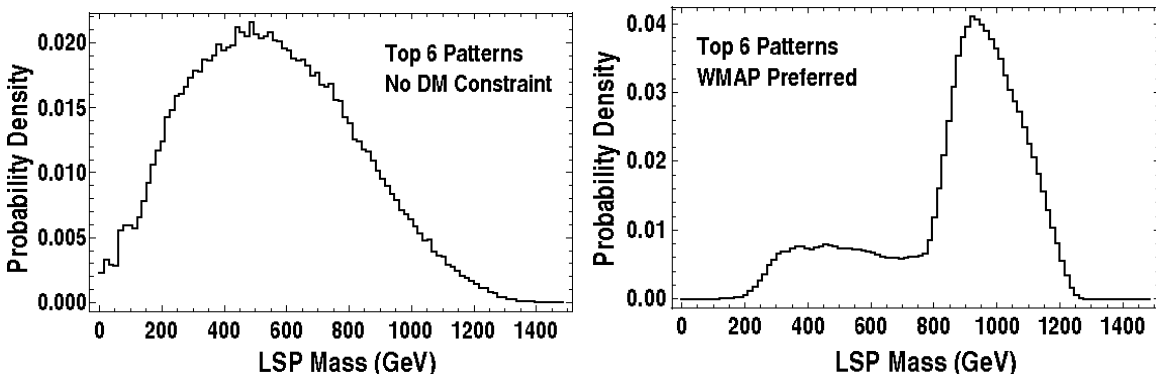


Figure 22: LSP mass distribution. We show the distribution of the neutralino LSP mass for the top six hierarchy patterns in DMM models, with no dark matter constraint (left panel) and the WMAP Preferred constraint (right panel).

The significance of the dark matter requirement should not be understated. Consider the case of Fig. 22, in which we plot the distribution in mass for the lightest neutralino for the aggregate set of our top six hierarchy patterns (Higgs LSP, mSP2, mSP2', mSP3, mSP3' and mSP6'). The left panel shows the distribution with absolutely no dark matter constraint imposed, revealing a general preference for masses of order a few hundred GeV with a wide distribution. In the right panel we have required the strict condition that the thermal relic abundance fall within the WMAP Preferred range. The probability density

immediately shifts to favor rather large masses for the LSP on the order of 1 TeV. The bulk of the shape is accounted for by the Higgs LSP pattern which is the dominant pattern in DMM, representing nearly half the models in the top-six patterns and 37% of the total models when this constraint is imposed. Patterns mSP2 and mSP2' also have distributions of LSP mass which are heavily concentrated near $m_{\chi_1^0} \simeq 1$ TeV. Most of the low-mass LSP models are those coming from patterns mSP3, mSP3' and mSP6' for which the LSP is predominantly bino-like, while the high mass models will have mixed neutralinos or predominantly Higgsino LSPs. These facts have large consequences for the direct and indirect detection of neutralino dark matter [34]. In particular, it is unlikely that the DMM model will produce a wino-like neutralino with a mass of 200 GeV or less which might explain the excess in positrons observed by PAMELA [35, 36].

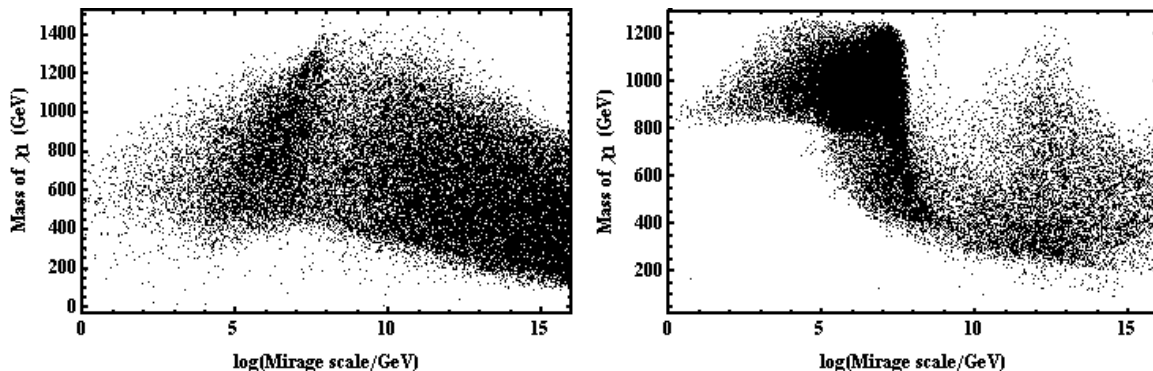


Figure 23: LSP mass versus mirage unification scale. We show the distribution of the LSP mass as a function of the mirage unification scale for the top six hierarchy patterns in DMM models, with no dark matter constraint (left panel) and the WMAP Preferred constraint (right panel).

As was demonstrated in Section 4.3, the wavefunction composition of the LSP is strongly correlated with the scale of mirage unification, defined in (2.7). Therefore imposition of a tight dark matter density requirement will preferentially select certain areas in the theoretical parameter space. This is illustrated in Fig. 23 for the combined set of top-six hierarchy patterns. Again, the left panel involves no dark matter requirement at all, while the right panel imposes the WMAP Preferred relic density constraint. While no strong correlations are evident in the former case, the latter case shows the clear transition at $M_{\text{mir}} \simeq 10^8$ GeV and the absence of low-mass LSPs for lower mirage scales.

The mirage scale itself is closely tied to the fundamental input parameter α_m which measures the relative contributions of anomaly and gravity mediation to the soft supersymmetry breaking. The mirage scale is much less sensitive to the value of α_g which compares the gauge mediation contribution to the bulk gravity contribution. This is illustrated for our top-six hierarchy patterns in Fig. 24 where both distributions require the WMAP Preferred relic density for the LSP. The distribution in α_m is the mirror image of the right panel in the previous figure: higher mirage unification scales correspond to lower values of α_m , while the bulk of the models lie in the region $1 \lesssim \alpha_m \lesssim 2$ where the unification scale is below 10^8 GeV. It is interesting that one of the *least* favorable regions for the model

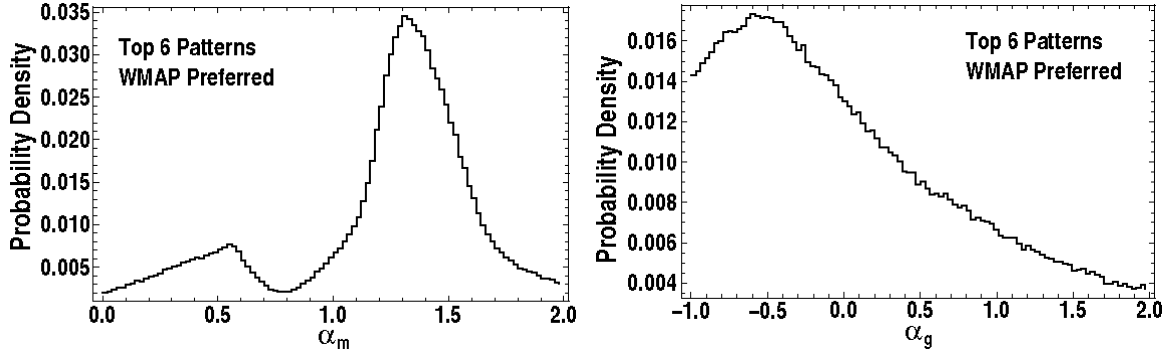


Figure 24: Distribution in input parameters α_m and α_g . We show the distributions of α_m (left panel) and α_g (right panel) for the top six hierarchy patterns in DMM models with the WMAP Preferred constraint.

set is the KKLT-limit of $\alpha_m = 1$, though lower values of $\alpha_m \sim 0.5$ which are typical of some heterotic constructions [37, 38] continue to be viable. The overall distribution in the variable α_g is rather broad, but clearly favors $\alpha_g < 0$ once the dark matter condition is imposed. This has model-building implications: negative values of this parameter favor stabilization mechanisms for the Standard Model singlet field X , which generates masses for the gauge-charged messenger fields, which involve higher-dimensional operators in the effective superpotential as opposed to non-perturbative stabilization mechanisms.

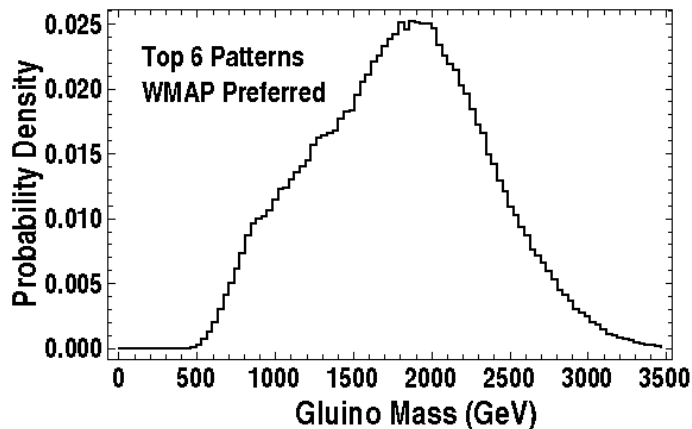


Figure 25: Distribution of gluino mass. We show the distribution of the gluino mass for the top six hierarchy patterns in DMM models with the WMAP Preferred constraint.

The vast majority of DMM model points involve a mirage unification scale below the (true) unification scale of 10^{16} GeV, which would be the scale of gaugino mass unification in mSUGRA. The lowering of the mirage unification scale from the mSUGRA limit results in a more compressed spectrum in the gaugino sector which distinguishes DMM models from mSUGRA models. The distinctive gaugino mass ratios of mSUGRA will be perturbed and there arises a greater possibility of mixed-composition lightest neutralino. Strategies

for measuring this deviation in the gaugino mass sector at the LHC have been developed elsewhere [39, 16]. A central question, however, is whether the relatively heavy spectrum implied by the large LSP mass will be accessible at the LHC. In minimal supergravity one typically expects the physical gluino mass to be 5 to 6 times larger than the mass of the LSP. In the DMM framework, this ratio can be significantly smaller, as seen in Section 4.3. The compression of the spectrum often implies a gluino mass roughly a factor of two times larger than the LSP mass, with gluinos and squarks very comparable in mass. Would such states be accessible at the LHC? An LSP of mass on the order of 1 TeV in the mSUGRA limit would be a disaster for the LHC since even 1 ab^{-1} of integrated luminosity at $\sqrt{s} = 14 \text{ TeV}$ would not be sufficient to discover a 5-6 TeV gluino [42]. But in the DMM model the typical gluino mass is in the 1-2 TeV range, and frequently much smaller. For cases in which $m_{\tilde{q}} \simeq m_{\tilde{g}}$, as in the DMM paradigm, gluinos in the TeV range are detectable with $1\text{-}2 \text{ fb}^{-1}$ of integrated luminosity, even at $\sqrt{s} = 7 \text{ TeV}$ [40, 41]. Heavier gluinos in the range $2 \text{ TeV} \lesssim m_{\tilde{g}} \lesssim 3 \text{ TeV}$ are still accessible at the LHC with 100 fb^{-1} of data at $\sqrt{s} = 14 \text{ TeV}$ [42]. As Fig. 25 displays for our six most common hierarchy patterns, the gluino mass distribution peaks just below $m_{\tilde{g}} = 2 \text{ TeV}$ and is well constrained to be below 3 TeV. This provides the exciting possibility that the rich structure of deflected mirage mediation could be probed at the LHC in the coming years.

Acknowledgments

The work of B.A. and B.D.N. is supported by the National Science Foundation Grant PHY-0653587. L.E. and Y.R. are supported by the U.S. Department of Energy grant DE-FG-02-95ER40896. The work of I.W.K. is supported by the U.S. Department of Energy grants DE-FG-02-95ER40899 and DE-FG-02-95ER40896.

A. DMM Parameters

The θ_i parameters, which appear in the mixed modulus-anomaly term in the soft scalar mass-squared parameters, are given by

$$\begin{aligned}
\theta_{Q,i} &= \frac{16}{3}g_3^2 + 3g_2^2 + \frac{1}{15}g_1^2 - 2(y_t^2 + y_b^2)\delta_{i3}, \\
\theta_{U,i} &= \frac{16}{3}g_3^2 + \frac{16}{15}g_1^2 - 4y_t^2\delta_{i3}, \quad \theta_{D,i} = \frac{16}{3}g_3^2 + \frac{4}{15}g_1^2 - 4y_b^2\delta_{i3}, \\
\theta_{L,i} &= 3g_2^2 + \frac{3}{5}g_1^2 - 2y_\tau^2\delta_{i3}, \quad \theta_{E,i} = \frac{12}{5}g_1^2 - 4y_\tau^2\delta_{i3}, \\
\theta_{H_u} &= 3g_2^2 + \frac{3}{5}g_1^2 - 6y_t^2, \quad \theta_{H_d} = 3g_2^2 + \frac{3}{5}g_1^2 - 6y_b^2 - 2y_\tau^2.
\end{aligned} \tag{A.1}$$

The $\dot{\gamma}'_i$ parameters are:

$$\begin{aligned}
\dot{\gamma}'_{Q,i} &= \frac{8}{3}b'_3g_3^4 + \frac{3}{2}b'_2g_2^4 + \frac{1}{30}b'_1g_1^4 - (y_t^2b_t + y_b^2b_b)\delta_{i3} \\
\dot{\gamma}'_{U,i} &= \frac{8}{3}b'_3g_3^4 + \frac{8}{15}b'_1g_1^4 - 2y_t^2b_t\delta_{i3}, \quad \dot{\gamma}'_{D,i} = \frac{8}{3}b'_3g_3^4 + \frac{2}{15}b'_1g_1^4 - 2y_b^2b_b\delta_{i3} \\
\dot{\gamma}'_{L,i} &= \frac{3}{2}b'_2g_2^4 + \frac{3}{10}b'_1g_1^4 - y_\tau^2b_\tau\delta_{i3}, \quad \dot{\gamma}'_{E,i} = \frac{6}{5}b'_1g_1^4 - 2y_\tau^2b_\tau\delta_{i3} \\
\dot{\gamma}'_{H_u} &= \frac{3}{2}b'_2g_2^4 + \frac{3}{10}b'_1g_1^4 - 3y_t^2b_t, \quad \dot{\gamma}'_{H_d} = \frac{3}{2}b'_2g_2^4 + \frac{3}{10}b'_1g_1^4 - 3y_b^2b_b - y_\tau^2b_\tau, \quad (\text{A.2})
\end{aligned}$$

where $b'_a = b_a + N$ ($a = 1, 2, 3$), and $b_{3,2,1} = -3, 1, 33/5$ are the MSSM beta functions (our convention is that $b'_a < 0$ for asymptotically free gauge theories).

The threshold effects for the soft scalar mass-squared parameters (see Eq. (2.6)) are given by

$$\begin{aligned}
\Delta m_Q^2 &= M_0^2 \left(\frac{8}{3}g_3^4 + \frac{3}{2}g_2^4 + \frac{1}{30}g_1^4 \right) N\tilde{\alpha}_m(1 + \alpha_g) \\
\Delta m_U^2 &= M_0^2 \left(\frac{8}{3}g_3^4 + \frac{8}{15}g_1^4 \right) N\tilde{\alpha}_m(1 + \alpha_g) \\
\Delta m_D^2 &= M_0^2 \left(\frac{8}{3}g_3^4 + \frac{2}{15}g_1^4 \right) N\tilde{\alpha}_m(1 + \alpha_g) \\
\Delta m_L^2 &= M_0^2 \left(\frac{3}{2}g_2^4 + \frac{3}{10}g_1^4 \right) N\tilde{\alpha}_m(1 + \alpha_g) = \Delta m_{H_u}^2 = \Delta m_{H_d}^2 \\
\Delta m_E^2 &= M_0^2 \frac{6}{5}g_1^4 N\tilde{\alpha}_m(1 + \alpha_g), \quad (\text{A.3})
\end{aligned}$$

where the gauge couplings are evaluated at the messenger scale, M_{mess} .

References

- [1] S. P. Martin, arXiv:hep-ph/9709356.
- [2] D. J. H. Chung, L. L. Everett, G. L. Kane, S. F. King, J. D. Lykken and L. T. Wang, Phys. Rept. **407**, 1 (2005) [arXiv:hep-ph/0312378].
- [3] B. C. Allanach *et al.*, in *Proc. of the APS/DPF/DPB Summer Study on the Future of Particle Physics (Snowmass 2001)* ed. N. Graf, Eur. Phys. J. C **25**, 113 (2002) [arXiv:hep-ph/0202233].
- [4] C. F. Berger, J. S. Gainer, J. L. Hewett and T. G. Rizzo, JHEP **0902**, 023 (2009) [arXiv:0812.0980 [hep-ph]].
- [5] D. Feldman, Z. Liu and P. Nath, Phys. Rev. Lett. **99**, 251802 (2007) [Erratum-ibid. **100**, 069902 (2008)] [arXiv:0707.1873 [hep-ph]].
- [6] D. Feldman, Z. Liu and P. Nath, Phys. Lett. B **662**, 190 (2008) [arXiv:0711.4591 [hep-ph]].
- [7] D. Feldman, Z. Liu and P. Nath, JHEP **0804**, 054 (2008) [arXiv:0802.4085 [hep-ph]].
- [8] L. L. Everett, I. W. Kim, P. Ouyang and K. M. Zurek, Phys. Rev. Lett. **101**, 101803 (2008) [arXiv:0804.0592 [hep-ph]].
- [9] L. L. Everett, I. W. Kim, P. Ouyang and K. M. Zurek, JHEP **0808**, 102 (2008) [arXiv:0806.2330 [hep-ph]].
- [10] S. Nakamura, K. i. Okumura and M. Yamaguchi, Phys. Rev. D **77**, 115027 (2008) [arXiv:0803.3725 [hep-ph]].
- [11] K. Choi, A. Falkowski, H. P. Nilles, M. Olechowski and S. Pokorski, JHEP **0411** (2004) 076 [arXiv:hep-th/0411066]; K. Choi, A. Falkowski, H. P. Nilles and M. Olechowski, Nucl. Phys. B **718** (2005) 113 [arXiv:hep-th/0503216].
- [12] K. Choi, K. S. Jeong and K. i. Okumura, JHEP **0509**, 039 (2005) [arXiv:hep-ph/0504037].
- [13] M. Endo, M. Yamaguchi and K. Yoshioka, Phys. Rev. D **72**, 015004 (2005) [arXiv:hep-ph/0504036]; A. Falkowski, O. Lebedev and Y. Mambrini, JHEP **0511**, 034 (2005) [arXiv:hep-ph/0507110]; H. Baer, E. Park, X. Tata and T. T. Wang, JHEP **0608**, 041 (2006) [arXiv:hep-ph/0604253], JHEP **0706**, 033 (2007) [arXiv:hep-ph/0703024]; K. Choi and H. P. Nilles, JHEP **0704**, 006 (2007) [arXiv:hep-ph/0702146]; K. Choi, K. Jeong, T. Kobayashi, and K. Okumura, Phys. Lett. B **633**, 355 (2006) [arXiv:hep-ph/0508029]; R. Kitano and Y. Nomura, Phys. Lett. B **631**, 58 (2005) [arXiv:hep-ph/0509039]; O. Lebedev, H. P. Nilles and M. Ratz, hep-ph/0511320; A. Pierce and J. Thaler, JHEP **0609**, 017 (2006) [arXiv:hep-ph/0604192]. K. Choi, K. Jeong, T. Kobayashi and K. Okumura, Phys. Rev. D **75**, 095012 (2007) [arXiv:hep-ph/0612258].
- [14] K. Choi, K. S. Jeong, S. Nakamura, K. I. Okumura and M. Yamaguchi, JHEP **0904**, 107 (2009) [arXiv:0901.0052 [hep-ph]].
- [15] M. Holmes and B. D. Nelson, JCAP **0907**, 019 (2009) [arXiv:0905.0674 [hep-ph]].
- [16] B. Altunkaynak, B. D. Nelson, L. L. Everett, I. W. Kim and Y. Rao, JHEP **1005**, 054 (2010) [arXiv:1001.5261 [hep-ph]].
- [17] S. Kachru, R. Kallosh, A. D. Linde and S. P. Trivedi, Phys. Rev. D **68**, 046005 (2003) [arXiv:hep-th/0301240].

- [18] A. Brignole, L. E. Ibanez and C. Munoz, Nucl. Phys. B **422**, 125 (1994) [Erratum-ibid. B **436**, 747 (1995)] [arXiv:hep-ph/9308271].
- [19] A. Djouadi, M. Drees and J. L. Kneur, JHEP **0603**, 033 (2006) [arXiv:hep-ph/0602001]; A. Djouadi, M. Drees and J. L. Kneur, JHEP **0108**, 055 (2001) [arXiv:hep-ph/0107316].
- [20] V. M. Abazov *et al.* [D0 Collaboration], Phys. Lett. B **660**, 449 (2008) [arXiv:0712.3805 [hep-ex]].
- [21] J. Alwall, M. P. Le, M. Lisanti and J. G. Wacker, Phys. Lett. B **666**, 34 (2008) [arXiv:0803.0019 [hep-ph]].
- [22] D. S. M. Alves, E. Izaguirre and J. G. Wacker, arXiv:1008.0407 [hep-ph].
- [23] E. Barberio *et al.* [Heavy Flavor Averaging Group (HFAG) Collaboration], arXiv:0704.3575 [hep-ex].
- [24] T. Aaltonen *et al.* [CDF Collaboration], Phys. Rev. Lett. **100**, 101802 (2008) [arXiv:0712.1708 [hep-ex]].
- [25] D. N. Spergel *et al.* [WMAP Collaboration], Astrophys. J. Suppl. **170**, 377 (2007) [arXiv:astro-ph/0603449].
- [26] J. Dunkley *et al.* [WMAP Collaboration], Astrophys. J. Suppl. **180**, 306 (2009) [arXiv:0803.0586 [astro-ph]].
- [27] D. Larson *et al.*, arXiv:1001.4635 [astro-ph.CO].
- [28] P. Salati, Phys. Lett. B **571**, 121 (2003) [arXiv:astro-ph/0207396]; M. Kamionkowski and M. S. Turner, Phys. Rev. D **42**, 3310 (1990);
- [29] D. Comelli, M. Pietroni and A. Riotto, Phys. Lett. B **571**, 115 (2003) [arXiv:hep-ph/0302080].
- [30] F. Rosati, Phys. Lett. B **570**, 5 (2003) [arXiv:hep-ph/0302159].
- [31] S. Profumo and P. Ullio, JCAP **0311**, 006 (2003) [arXiv:hep-ph/0309220]; R. Catena, N. Fornengo, A. Masiero, M. Pietroni and F. Rosati, Phys. Rev. D **70**, 063519 (2004) [arXiv:astro-ph/0403614]; A. Masiero and F. Rosati, arXiv:astro-ph/0501571; C. Pallis, JCAP **0510**, 015 (2005) [arXiv:hep-ph/0503080], Nucl. Phys. B **751**, 129 (2006) [arXiv:hep-ph/0510234]; D. J. H. Chung, L. L. Everett and K. T. Matchev, Phys. Rev. D **76**, 103530 (2007) [arXiv:0704.3285 [hep-ph]]; D. J. H. Chung, L. L. Everett, K. Kong and K. T. Matchev, JHEP **0710**, 016 (2007) [arXiv:0706.2375 [hep-ph]].
- [32] N. Arkani-Hamed, A. Delgado and G. F. Giudice, Nucl. Phys. B **741**, 108 (2006) [arXiv:hep-ph/0601041].
- [33] A. Birkedal-Hansen and B. D. Nelson, Phys. Rev. D **64**, 015008 (2001) [arXiv:hep-ph/0102075].
- [34] A. Birkedal-Hansen and B. D. Nelson, Phys. Rev. D **67**, 095006 (2003) [arXiv:hep-ph/0211071].
- [35] O. Adriani *et al.* [PAMELA Collaboration], Nature **458**, 607 (2009) [arXiv:0810.4995 [astro-ph]].

- [36] P. Grajek, G. Kane, D. Phalen, A. Pierce and S. Watson, Phys. Rev. D **79**, 043506 (2009) [arXiv:0812.4555 [hep-ph]]; G. Kane, R. Lu and S. Watson, Phys. Lett. B **681**, 151 (2009) [arXiv:0906.4765 [astro-ph.HE]]; D. Feldman, Z. Liu, P. Nath and B. D. Nelson, Phys. Rev. D **80**, 075001 (2009) [arXiv:0907.5392 [hep-ph]]; D. Feldman, G. Kane, R. Lu and B. D. Nelson, Phys. Lett. B **687**, 363 (2010) [arXiv:1002.2430 [hep-ph]].
- [37] M. K. Gaillard, B. D. Nelson and Y. Y. Wu, Phys. Lett. B **459**, 549 (1999) [arXiv:hep-th/9905122].
- [38] M. K. Gaillard and B. D. Nelson, Int. J. Mod. Phys. A **22**, 1451 (2007) [arXiv:hep-th/0703227].
- [39] B. Altunkaynak, P. Grajek, M. Holmes, G. Kane and B. D. Nelson, JHEP **0904**, 114 (2009) [arXiv:0901.1145 [hep-ph]].
- [40] H. Baer, V. Barger, A. Lessa and X. Tata, JHEP **1006**, 102 (2010) [arXiv:1004.3594 [hep-ph]].
- [41] B. Altunkaynak, M. Holmes, P. Nath, B. D. Nelson and G. Peim, arXiv:1008.3423 [hep-ph].
- [42] H. Baer, V. Barger, A. Lessa and X. Tata, JHEP **0909**, 063 (2009) [arXiv:0907.1922 [hep-ph]].